Computers and Structures 333 (2026) 108441

Contents lists available at ScienceDirect

Computers and Structures

journal homepage: www.elsevier.com/locate/cas

# Exact Numerical Time Integration (ENTI) of dynamic equations of motion for discretized systems subjected to Moving Load

Michele Guerini [a], Rosalba Ferrari [a,*], Giuseppe Cocchetti [b,a], Egidio Rizzi [a]

[a] University of Bergamo, Department of Engineering and Applied Sciences, viale G. Marconi 5, I-24044 Dalmine (BG), Italy
[b] Politecnico di Milano, Department of Civil and Environmental Engineering, piazza L. da Vinci 32, I-20133 Milano, Italy

ARTICLE INFO

*Keywords:*
Linear Time-Invariant (LTI) dynamic system
Discretized model
Exponential matrix
Exact integration
Moving Load (ML)
Historic iron arch bridge beam

ABSTRACT

This study presents an Exact Numerical Time Integration (ENTI) method, formulated within the exponential integrator framework, to perform "exact" dynamic analyses of discretized Linear Time-Invariant systems, toward the correct evaluation of displacement, velocity, and acceleration response variables. The method guarantees an exact time evolution of the state variables through the governing state-transition matrix expressed by an exponential matrix. One main novelty of the method lies in replacing numerical approximations of the state-transition matrix with explicit, closed-form analytical expressions of the exponential matrix for both undamped and classically damped systems. Its capabilities are illustrated for a constant-magnitude Moving Load (ML) problem on a discretized Euler-Bernoulli beam Finite Element Method (FEM) model. The Moving Load, travelling at constant speed, is modelled with equivalent nodal forces. Then, the underlying convolution integral in the general solution is solved in closed-form, thereby entirely eliminating time-discretization errors and leaving the solution solely affected by machine-precision round-off. Finally, the method is applied to a one-dimensional FEM model of the upper continuous beam of historic Paderno d'Adda Bridge (1889), under ML. Comparisons with conventional time-integration schemes show significant discrepancies, especially in acceleration responses, while ENTI remains accurate, reliable, and computationally efficient, regardless of the adopted time-step sampling.

## 1. Introduction

This paper presents a novel formulation for the dynamic analysis of given discretized structural systems, aiming at providing both "exact" time integration and computational efficiency. The method, herein named Exact Numerical Time Integration (ENTI), has been developed to solve the dynamic equations of motion, in a state-space, first-order differential representation, governing structural systems modelled as Linear Time-Invariant (LTI) systems, which may come out from a multi-degree of freedom description or discretization through techniques like the Finite Element Method (FEM).

The proposed formulation shall be grounded on the general framework of "exponential integrators", and shares the use of the exponential matrix, which shall constitute the fundamental operator to solve the first-order equations of motion for LTI systems. Specifically focusing on the dynamic context of structures, the exponential matrix is herein computed in closed-form, for undamped and classically damped systems, thus providing a numerically exact solution, limited only by machine precision.

To illustrate the specific potentialities of this method, the dynamic problem of structures subjected to a constant-magnitude Moving Load (ML) travelling at uniform speed along the system is investigated, and the resulting dynamic variables calculated by the ENTI method are compared with those solved using common numerical schemes. This comparison aims at demonstrating that, unlike black-box approaches affected by algorithmic time-integration errors, the proposed method delivers a numerically exact solution, specifically referring to accelerations, which may often constitute the primary variables acquired in experimental dynamics, and likely the most sensitive to numerical approximations.

In summary, the main novel contributions of the proposed ENTI framework lie in:

1. Exact and efficient convolution integration: the spatial-temporal convolution integral governing constant-speed moving nodal forces is fully analytically solved, through an efficient recursive formulation, completely bypassing numerical quadrature

* Corresponding author.
*Email address:* rosalba.ferrari@unibg.it (R. Ferrari).

https://doi.org/10.1016/j.compstruc.2026.108441
Received 27 May 2026; Accepted 5 September 2026
Available online 20 October 2026
0045-7949/© 2026 The Authors. Published by Elsevier Ltd. This is an open access article under the CC BY-NC-ND license (http://creativecommons.org/licenses/by-nc-nd/4.0/).

rules and thereby entirely eliminating time-discretization and truncation errors.
2. Closed-form exponential matrix: the proposed ENTI method derives explicit, closed-form expressions for the state-transition matrix for both undamped and classically damped LTI structural systems, thus without relying on approximations, e.g., as Padé or Krylov.
3. Exact benchmark for discretized dynamic response variables: the formulation provides an exact benchmark for all state response variables (displacement, velocity, and notably acceleration), proving that standard time-stepping schemes may suffer from significant numerical errors, especially in acceleration predictions, regardless of the adopted time step.
4. Extensibility to general external force terms: the underlying mathematical structure of the method is not restricted to Moving Load problems, but may allow for straightforward extensions to broader classes of space-time varying forcing terms, including for input with high-frequency content (e.g., Heaviside step functions, triangular pulses, impact loadings, etc.).

As a matter of fact, the development of the present ENTI method originated from specific needs arising in the field of Structural Health Monitoring (SHM), and particularly within the framework of creating a reliable digital twin replication of historic Paderno d'Adda Bridge, also known as San Michele Bridge (1889) [1,2], an impressive iron arch bridge that still plays a key role in the local railway and transportation network of Lombardia, northern Italy, by connecting the provinces of Lecco and Bergamo. Within the broader scope of SHM, one possible strategy for assessing the health condition of a structure is indeed that of assembling a loyal digital twin replication [3], equipped with analytical tools capable of simulating and predicting its dynamic response under various types of loads and excitations, with the goal of exploring current and potential future utilization scenarios, of the attentioned construction. Such digital platforms are also designed to perform parameter identification, model updating, and potential damage estimation [4–6], which shall be essential to support informed maintenance planning.

Beyond SHM applications, there is an increasing interest in mechanical analyses addressing both general and specific aspects of structural dynamic behaviour, such as vehicle-structure interaction [7–10] and vibration response under ML conditions [11–13]. Reliable simulated data obtained through consistent numerical formulations may be integrated into response reconstruction strategies within SHM frameworks, particularly when measurement data are not available, corrupted during transmission, or when the monitored structure is characterized by sparse sensing [14,15]. In such cases, advanced analysis tools, including data-fusion techniques, may play a crucial role in mitigating these limitations [16,17].

Typically, the simulated data of interest may include displacement, velocity, and acceleration response signals, whose comparison with real structural responses represents a rather challenging task, especially in dynamic scenarios involving MLs. In these cases, the equations of motion are difficult to accurately be solved, as the applied excitation varies simultaneously in both time and space, making it complex to achieve a close agreement with experimental data, particularly in terms of velocity and, most of all, acceleration responses.

For discretized structures, the equations of motion may traditionally be solved using numerical time-integration methods, such as well-known Newmark, Wilson-$\theta$, HHT-$\alpha$ methods, which are widely implemented in commercial software for their robustness and "black-box" nature. The origin of these classical approaches shall date back to 1959, when Nathan M. Newmark introduced what later became known as the Newmark method [18]. Subsequently, new algorithms were proposed, such as the Wilson-$\theta$ method (1968) [19], designed for the dynamic stress analysis of underground structures. Stability and accuracy analyses by Bathe and Wilson (1972) [20] demonstrated that both the Newmark and Wilson-$\theta$ methods shall yield accurate results for certain types of problems, with the latter being a single-step, implicit, and unconditionally stable method for Wilson-$\theta$ parameter $\theta > 1.37$.

Later developments introduced a new family of single-step, implicit, unconditionally stable, and second-order accurate algorithms, namely the HHT-$\alpha$ method (1977, 1983) [21,22] and the Generalized-$\alpha$ (1993) [23] method. These are often referred to as equilibrium averaging methods, since they average the dynamic equations, and can be tuned to control the level of numerical dissipation. More recent contributions, such as those by K.J. Bathe and co-workers, e.g., Bathe and Baig (2005) [24] and Bathe and Noh (2012) [25], have continued to refine these approaches, yet all of them sharing an inherent numerical approximation in the time-integration process. Also, overshooting phenomena in time-integration methods in linear elastodynamics, by overlooking some specific numerical issues, have been investigated in Benítez and Montáns (2013) [26].

In contrast, the present ENTI method aims at achieving an "exact" numerical time integration for discretized structural systems, thus providing a potential breakthrough in the simulation accuracy and computational reliability of dynamic structural analyses. The ENTI method is formulated in a state-space framework, and this representation reduces the order of the governing differential equations, from a second-order to a first-order system, allowing the underlying convolution integral to be solved in closed form, specifically when a ML problem is herein considered. The method involves the evaluation of an exponential matrix and thus shall belong, in essence, to the broader class of "exponential integrators". Such approaches have successfully been applied in several areas of research, even beyond the structural dynamics context [27], and including e.g., reaction-advection-diffusion problems, mathematical finance, classical and quantum molecular dynamics, Schrödinger and Maxwell equations, for the regularization of ill-posed problems. A comprehensive overview on these applications may be found in [28].

Several exponential integration schemes have been proposed over the years [29–46,55,56]. To the best of the authors' knowledge, the first shall have been introduced in 1958 by Hersch [29], who observed that traditional finite-difference schemes do not provide exact solutions even when the governing linear differential equations with constant coefficients can be analytically solved. To overcome this limitation, integration schemes yielding exact solutions for such systems were developed. Conventional numerical integration methods are often ineffective in problems characterized by rapidly varying transients, for which the selection of an appropriate time step becomes particularly difficult [30].

Further advances were made by Pope in 1963 [31], who proposed an exponential-based formulation exhibiting superior stability properties for relatively large time steps, thereby allowing for a significant reduction in computational cost. Additional contributions demonstrating the advantages of exponential integrators were provided, e.g., by Loffeld and Tokman [32,33]. Their work focused on the numerical integration of large, stiff systems of ordinary differential equations with non-symmetric Jacobians, for which implicit Newton-Krylov methods [34] are typically adopted alongside carefully constructed preconditioners. In their study, Krylov-based exponential integrators were compared with traditional implicit and explicit schemes, over a wide range of test cases, providing one of the first quantitative assessments of the computational benefits of exponential integration methods, and highlighting the efficiency of the exponential propagation Runge-Kutta (EpiRK) methods of the fifth order.

With reference to structural dynamics, early attempts to overcome the time-step limitations of classical direct integration methods were proposed by Lin et al. [35], through the High Precision Direct (HPD) method. In this approach, the external loading is expressed in terms of linear, sinusoidal, or Fourier series expansions, and the dynamic equations of motion are solved using the exponential matrix, computed via a truncated Taylor series. These developments anticipated the emergence of more advanced exponential schemes, specifically designed to enhance stability and accuracy, when dealing with oscillatory responses.

Later, Michels et al. [36] investigated the application of exponential integrators to the efficient solution of stiff second-order differential equations arising in the simulation of deformable bodies, such as fibres, textiles, and solids. Unlike explicit schemes, exponential integrators are not constrained by high-frequency modes, and, in contrast to implicit schemes, avoid the introduction of artificial numerical dissipation. The authors also proposed a corotational extension that enables the simulation of large rotations by aligning the coordinate system with the deforming object, thus avoiding costly nonlinear computations. The use of filter functions and Krylov subspace techniques further improved the stability and efficiency of the matrix function evaluations. This formulation permits larger time steps, ensures better energy conservation, and enables near real-time performance, making it highly competitive for stiff mechanical systems.

In the field of elastodynamics, Pari et al. [37] recently proposed a Magnus-based exponential propagator, in which the second-order elastodynamic equations are transformed into a first-order system and solved via a truncated Magnus expansion [38,39]. By employing adaptive Krylov subspace projections, the proposed method achieves a second-order convergence, while preserving both energy and symplectic properties. Owing to the inherent characteristics of exponential integrators, this approach allows the use of significantly larger time steps than conventional time-integration schemes, resulting in computational speed-ups of up to two orders of magnitude in nonlinear applications.

In the literature, numerous strategies have been proposed for the pertinent evaluation and approximation of the involved exponential matrix [40–44], with the primary focus placed on the efficient computation of this operator. For example, based on a Padé approximation, a single-step high-order implicit time-integration scheme was proposed by Song et al. [46] to solve transient and wave propagation problems. A notable feature of this method is that it does not require any direct inversion of the mass matrix.

In contrast, the objective of the present work is to achieve an exact evaluation of the dynamic response, specifically that of a discrete one-dimensional multi-supported beam subjected to a ML travelling at constant speed and with constant magnitude. The structural system is discretized using Euler-Bernoulli FEs and assumed to be a Linear Time-Invariant system, and the ML is represented through equivalent nodal forces, resulting in a third-order polynomial expression in space [13]. This exact state-space formulation aims at bridging classical ML theory with recent FEM frameworks. Historically, the dynamic response of structures under travelling loads has posed significant analytical and computational challenges, as comprehensively treated in the book of Fryba (1999) [47]. This field, still under active investigation, due to various growing interests in different engineering scenarios, like for the analysis of bridges and by Structural Health Monitoring approaches, has also seen advances in FEM modelling, including for novel formulations for beam dynamics (see, e.g., Santos (2024) [48], in the present journal, where time integration has been carried out by a classical Newmark method). By combining a ML problem for a discretized structural model with an exponential integration approach, the proposed ENTI method seeks to deliver an exact and computationally efficient tool, within the broader family of state-space exponential integrators (see Hochbruck and Ostermann 2010 [28]).

The novelty of the herein proposed approach lies in the specific combination of an accurate modelling of the ML and the development of an original exponential integration scheme that yields an exact solution of the equations of motion, with numerical round-off errors arising only from machine precision. The displacement, velocity, and, most importantly, acceleration responses obtained using the proposed ENTI method are compared with those computed by classical numerical integration schemes, with the aim of highlighting the differences induced by conventional numerical time-stepping algorithms.

Notice that the present exact (time-integration) approach is fully original, though in principle belonging to the family of so-called exponential integrators, and shall anyway represent a further consistent alternative to other approaches that have put forward exact integration strategies, for instance by Laplace transformation, even in different mechanical contexts (e.g., by Beskos et al. [49–53] and Spyrakos et al. [53,54]). Without taking out merits to such valuable methodologies, the present procedure is definitely a purely analytical one, in delivering exact results, once the integration linked to the excitation term can analytically be performed, as in the case considered in the paper, in that no numerical truncation errors are linked to numerical handling, except of course for the inherent limits of machine precision. As such, notice that convergence studies or demonstrations on convergence rates are not pertinent to the present context, as instead shall be typical of classical numerical time-integration strategies. Moreover, the superiority of the present exact evaluation versus classical alternative numerical time-integration schemes is much analyzed and revealed in the paper.

Finally, it should be observed that, although the present ENTI method provides an exact time-domain solution of the dynamic equations of motion for a discretized system, the intrinsic discretization errors, arising from a discretization process of a continuum problem, cannot obviously be avoided. Nevertheless, the ENTI time-integration method may be adopted to benchmark problems that may possess a known analytical (continuum) solution. In this framework, the inherent time-integration error is completely eliminated; consequently, the discrepancy between an analytical solution and the ENTI solution can be utilized to deeply understand the effects of spatial-discretization errors, without any confounding numerical damping or period elongation from time-stepping algorithms arising from standard numerical time integration. On the other hand, due to the extendibility of the ENTI method to intrinsically discrete systems (e.g., lumped systems), typically being defined by given mass, damping and stiffness matrices, the ENTI time-integration method yields exact results in both space and time.

The paper is organized as follows. Section 2 introduces the general formulation of the present ENTI method and its application to the solution of the dynamic equations of motion of a discretized structural model subjected to ML. Section 3 outlines the computational strategy and the corresponding (MATLAB) implementation of the proposed ENTI method. The case study, consisting of a one-dimensional FEM representation of the upper continuous beam of the Paderno d'Adda Bridge (1889), is presented in Section 4, where the main results obtained using the ENTI method are discussed and compared with those produced by conventional time-integration schemes. Finally, Section 5 summarises the main findings and conclusions of the present investigation.

## 2. Exact Numerical Time Integration (ENTI) method

The ENTI method is herein proposed to solve systems of second-order Ordinary Differential Equations (ODEs) characterized by constant coefficients as typical of discrete, Linear Time-Invariant (LTI) structural systems. Specifically, second-order ODEs systems are largely employed to formulate structural dynamics problems, whose unknowns are displacement, velocity and acceleration variables. For these problems, the system may be represented through a discrete model, i.e., a system endowed with a finite number of Degrees Of Freedom (DOFs). Such a model may be an intrinsic Multi-DOF (MDOF) system or the result of the discretization of a continuous system, through computational procedures such as the FEM. Through such a discrete representation, the equations of motion may conveniently be expressed in matrix form, relating the DOFs' displacements, velocities, and accelerations to external actions.

Accordingly, the second-order differential dynamic equations of motion of a LTI structural system may classically be expressed as:

$$\mathbf{M}\ddot{\mathbf{u}} + \mathbf{C}\dot{\mathbf{u}} + \mathbf{K}\mathbf{u} = \mathbf{F}(t) \tag{1}$$

where $\mathbf{M}$, $\mathbf{C}$, and $\mathbf{K}$ represent the constant mass, damping, and stiffness matrices of the dynamic system, respectively ($n \times n$ matrices); $\mathbf{u}$, $\dot{\mathbf{u}}$, and $\ddot{\mathbf{u}}$ the displacement, velocity, and acceleration vectors ($n \times 1$, being $n$ the number of DOFs); $\mathbf{F}(t)$ the time-dependent force vector ($n \times 1$).

### 2.1. Preliminary operations to derive the ENTI method

The analytical determination of the particular solution of Eq. (1) is often mathematically challenging, especially when force term $\mathbf{F}(t)$ may involve non-elementary functions. To ease the evaluation of the solution, a common strategy contemplates the reduction of the second-order system, Eq. (1), into an equivalent first-order system, often referred to as a state-space representation, and subsequently attempt the derivation of the solution for this reduced-order system. By solving this equivalent system, the solution may eventually be mapped back to all the original second-order variables, namely DOFs' displacements, velocities, and accelerations.

#### 2.1.1. State-space representation

Typically, this order reduction is achieved by collecting $(n \times 1)$ displacements $\mathbf{u}$ and velocities $\dot{\mathbf{u}}$ into a state vector $\mathbf{z}$ whose dimensions become $(2n \times 1)$. Therefore, its derivative $\dot{\mathbf{z}}$ comprises velocities $\dot{\mathbf{u}}$ and accelerations $\ddot{\mathbf{u}}$ vectors, respectively:

$$\mathbf{z} = \begin{bmatrix} \mathbf{u} \\ \dot{\mathbf{u}} \end{bmatrix}, \quad \dot{\mathbf{z}} = \begin{bmatrix} \dot{\mathbf{u}} \\ \ddot{\mathbf{u}} \end{bmatrix} \tag{2}$$

Consequently, Eq. (1) may be reorganized according to state vectors $\mathbf{z}$ and $\dot{\mathbf{z}}$ as follows:

$$\begin{bmatrix} \mathbf{I} & \mathbf{0} \\ \mathbf{0} & \mathbf{M} \end{bmatrix} \begin{bmatrix} \dot{\mathbf{u}} \\ \ddot{\mathbf{u}} \end{bmatrix} + \begin{bmatrix} \mathbf{0} & -\mathbf{I} \\ \mathbf{K} & \mathbf{C} \end{bmatrix} \begin{bmatrix} \mathbf{u} \\ \dot{\mathbf{u}} \end{bmatrix} = \begin{bmatrix} \mathbf{0} \\ \mathbf{F}(t) \end{bmatrix} \tag{3}$$

leading to a first-order system of $2n$ dynamic equations, where $\mathbf{0}$ and $\mathbf{I}$ represent $(n \times n)$ zero and identity matrices, respectively.

Pre-multiplying by the inverse of the first block matrix (assuming matrix $\mathbf{M}$ to be invertible), Eq. (3) becomes:

$$\begin{bmatrix} \dot{\mathbf{u}} \\ \ddot{\mathbf{u}} \end{bmatrix} + \begin{bmatrix} \mathbf{0} & -\mathbf{I} \\ \mathbf{M}^{-1}\mathbf{K} & \mathbf{M}^{-1}\mathbf{C} \end{bmatrix} \begin{bmatrix} \mathbf{u} \\ \dot{\mathbf{u}} \end{bmatrix} = \begin{bmatrix} \mathbf{0} \\ \mathbf{M}^{-1}\mathbf{F}(t) \end{bmatrix} \tag{4}$$

Then, it is possible to define the following core arrays of the present state-space representation:

$$\mathbf{S} = \begin{bmatrix} \mathbf{0} & -\mathbf{I} \\ \mathbf{M}^{-1}\mathbf{K} & \mathbf{M}^{-1}\mathbf{C} \end{bmatrix}, \quad \mathbf{T}(t) = \begin{bmatrix} \mathbf{0} \\ \mathbf{M}^{-1}\mathbf{F}(t) \end{bmatrix} \tag{5}$$

so that the system may compactly be written as a linear first–order system of $2n$ ODEs:

$$\dot{\mathbf{z}} + \mathbf{S}\mathbf{z} = \mathbf{T}(t) \tag{6}$$

Herein, $\mathbf{S}$ is the matrix that governs the transition of state, including mass, damping and stiffness properties of a discrete or discretized model and $\mathbf{T}(t)$ is the equivalent force term for the first-order system. Both matrix $\mathbf{S}$ and force term $\mathbf{T}(t)$ will play a central role in the sections that follow, and in particular in the context of the modelization of a ML problem.

#### 2.1.2. Exponential matrix definition and properties

Before proceeding with the derivation of the solution of Eq. (6), it may be useful to introduce the exponential matrix operator, and some of its key properties, which will be utilized in the subsequent steps. In general, this operator is essential for solving systems of linear ODEs, as it generalizes the concept of a scalar exponential to a matrix context.

Given a square matrix $\mathbf{A}$, its exponential matrix, denoted as $e^{\mathbf{A}}$, may be defined by the following power series expansion [57–60]:

$$e^{\mathbf{A}} = \sum_{k=0}^{\infty} \frac{1}{k!}\mathbf{A}^k \tag{7}$$

The exponential matrix of $\mathbf{A}$ exhibits the following properties:

(i) *Diagonal matrices*: if matrix $\mathbf{A}$ is assumed to be diagonal, $\mathbf{A} = \mathrm{diag}(a_1, \dots, a_n)$, consequently $e^{\mathbf{A}} = \mathrm{diag}(e^{a_1}, e^{a_2}, \dots, e^{a_n})$ is diagonal as well;

(ii) *Commutativity and Inverse*: if two square matrices $\mathbf{A}$ and $\mathbf{B}$ commute ($\mathbf{AB} = \mathbf{BA}$), then $e^{\mathbf{A}+\mathbf{B}} = e^{\mathbf{A}}e^{\mathbf{B}}$; as a corollary, $e^{\mathbf{A}}$ is always invertible and $\left(e^{\mathbf{A}}\right)^{-1} = e^{-\mathbf{A}}$;

(iii) *Differentiation*: term $e^{\mathbf{A}t}$ is differentiable with respect to variable $t$, and its derivative is expressed as $\mathbf{A}e^{\mathbf{A}t} = e^{\mathbf{A}t}\mathbf{A}$. This highlights that matrix $\mathbf{A}$ and its exponential matrix $e^{\mathbf{A}}$ or $e^{\mathbf{A}t}$ always commute, a property that directly derives from the power series definition in Eq. (7), as $\mathbf{A}$ commutes with any of its own powers;

(iv) *Similarity Transformation*: if matrices $\mathbf{A}$ and $\mathbf{B}$ are similar, by means of a similarity matrix $\mathbf{P}$ (for instance, a modal matrix), then also $e^{\mathbf{A}}$ and $e^{\mathbf{B}}$ are similar. Specifically, if $\mathbf{A} = \mathbf{P}^{-1}\mathbf{B}\mathbf{P}$, $\mathbf{A}^k = \mathbf{P}\mathbf{B}^k\mathbf{P}^{-1}$, which implies $e^{\mathbf{A}} = \mathbf{P}^{-1}e^{\mathbf{B}}\mathbf{P}$.

#### 2.1.3. General solution of the first-order ODEs system

To handle Eq. (6), both left and right-hand sides are premultiplied by the (always non singular) exponential matrix of argument $\mathbf{S}t$:

$$e^{\mathbf{S}t}\dot{\mathbf{z}} + e^{\mathbf{S}t}\mathbf{S}\mathbf{z} = e^{\mathbf{S}t}\mathbf{T}(t) \tag{8}$$

By virtue of property (iii), the left-hand side of Eq. (8) can be identified as the total derivative of product $e^{\mathbf{S}t}\mathbf{z}$. Indeed, according to the product rule for derivatives, the first term on the left-hand-side represents the product between $e^{\mathbf{S}t}$ and the derivative of $\mathbf{z}$, while the second term the product between the derivative of $e^{\mathbf{S}t}$ and $\mathbf{z}$. Therefore, Eq. (8) becomes:

$$\frac{\mathrm{d}}{\mathrm{d}t}\left(e^{\mathbf{S}t}\mathbf{z}\right) = e^{\mathbf{S}t}\mathbf{T}(t) \tag{9}$$

To solve for $\mathbf{z}(t)$, both sides of the differential system are integrated over a given time interval $[t_n,\ t]$, where $t_n$ may represent an initial time instant:

$$\int_{t_n}^{t} \frac{\mathrm{d}}{\mathrm{d}\tau}\left(e^{\mathbf{S}\tau}\mathbf{z}(\tau)\right)\mathrm{d}\tau = \int_{t_n}^{t} e^{\mathbf{S}\tau}\mathbf{T}(\tau)\mathrm{d}\tau \tag{10}$$

By the Fundamental Theorem of Calculus, the left-hand side of Eq. (10) is evaluated over the integral limits $t$ and $t_n$, namely

$$\left[e^{\mathbf{S}\tau}\mathbf{z}(\tau)\right]_{t_n}^{t} = e^{\mathbf{S}t}\mathbf{z}(t) - e^{\mathbf{S}t_n}\mathbf{z}(t_n) \tag{11}$$

Consequently, in order to isolate state vector $\mathbf{z}(t)$, Eq. (10) is premultiplied by $e^{-\mathbf{S}t}$, taking advantage of the property of Commutativity and Inverse of the exponential matrix (ii), where $e^{-\mathbf{S}t}e^{\mathbf{S}t} = \mathbf{I}$ and $e^{-\mathbf{S}t}e^{\mathbf{S}t_n} = e^{-\mathbf{S}(t-t_n)}$, leading to the following formal expression of the general solution of the first-order ODEs system:

$$\mathbf{z}(t) = e^{-\mathbf{S}(t-t_n)}\mathbf{z}(t_n) + \int_{t_n}^{t} e^{-\mathbf{S}(t-\tau)}\mathbf{T}(\tau)\mathrm{d}\tau \tag{12}$$

where the first term refers to the homogeneous solution and the second one to the particular integral associated to $\mathbf{T}(t)$.

Typically, the solution expressed by Eq. (12) is evaluated at various discrete time instants along the whole time history $\{t_0, t_1, \dots, t_{N-1}, t_N\}$, where $t_N$ is the last time instant, with a possibly time-varying interval defined as:

$$\Delta t_n = t_{n+1} - t_n \tag{13}$$

To facilitate a recursive formulation, based on the information acquired at a previous time step, variable $\tau$, ranging between $t_n$ and $t_{n+1}$, is expressed as $\tau = t_n + r$, where $r \in [0, \Delta t_n]$ represents the local time variable within the time step. Consequently, to evaluate Eq. (12) at time instant $t_{n+1}$, integration variable $\tau$ may be replaced by $t_n + r$, leading to

new integration limits 0 and $\Delta t_n$ in variable $r$, and $t_{n+1} - \tau = \Delta t_n - r$. Then, factoring out constant term $e^{-\mathbf{S}\Delta t_n}$ from the integral, recursive solution $\mathbf{z}(t)$ becomes:

$$\mathbf{z}(t_{n+1}) = e^{-\mathbf{S}\Delta t_n}\mathbf{z}(t_n) + e^{-\mathbf{S}\Delta t_n}\int_0^{\Delta t_n} e^{\mathbf{S}r}\mathbf{T}(t_n + r)\mathrm{d}r \tag{14}$$

In general, to investigate complex transients or specific physical phenomena, a finer time resolution may be preferred only for a specific duration, to ensure accuracy in the final sampling representation. However, the standard approach for many structural applications may consider a uniform time interval $\Delta t_n = \Delta t$, ensuring a simplification of the recursive formulation, since exponential matrix $e^{-\mathbf{S}\Delta t}$ may be computed only at once, at the beginning of the formulation, outside the loop over the various time steps.

Finally, the physical variables of interest, displacements $\mathbf{u}$, velocities $\dot{\mathbf{u}}$, and accelerations $\ddot{\mathbf{u}}$, are formally retrieved out of the state-space representation in Eq. (6), through response vector $\mathbf{z}$, by means of two selection matrices, $\mathbf{L}_1$ and $\mathbf{L}_2$, of dimensions $n \times 2n$:

$$\mathbf{L}_1 = [\mathbf{I} \quad \mathbf{0}], \quad \mathbf{L}_2 = [\mathbf{0} \quad \mathbf{I}] \tag{15}$$

namely:

$$\mathbf{u} = \mathbf{L}_1\mathbf{z} \tag{16a}$$

$$\dot{\mathbf{u}} = \mathbf{L}_2\mathbf{z} \tag{16b}$$

$$\ddot{\mathbf{u}} = \mathbf{L}_2\dot{\mathbf{z}} = \mathbf{L}_2\left(-\mathbf{S}\mathbf{z} + \mathbf{T}(t)\right) \tag{16c}$$

At this stage, the formulation remains in its general form, as external force vector $\mathbf{F}(t)$ of Eq. (1), and consequently known term $\mathbf{T}(t)$ in Eq. (6), have not yet been specified. Within the proposed framework, the closed-form evaluation of the convolutional integral in Eq. (12) (i.e., its equivalent form in Eq. (14)) is strictly dependent on the mathematical nature of the external excitation.

It should be noted that the applicability of the ENTI method is wholly general, and not restricted to models obtained from a FEM discretization. In that case, the spatial domain discretization (e.g., via FEM) inherently introduces spatial approximations into continuum problems. While the ENTI method guarantees an exact time integration of the resulting discretized equations of motion, intrinsic spatial discretization errors may not be avoided. Although the following section will derive the problem formulation specifically for a FEM model subjected to Moving Load, the method shall remain valid for any discrete MDOF system. Regardless of the system's origin, if the forcing function is expressed through a set of basis functions, such as polynomials, sinusoids, or their combinations, the ENTI method shall enable an exact integration within the time step, independently on its size, thus avoiding truncation errors typical of conventional step-by-step numerical integrators, as well as quadrature approximations that often affect other exponential integrators. Furthermore, since the state-transition matrix, herein computed in closed-form, preserves the structural system's full eigenspectrum without introducing artificial dissipation, high-frequency modal contributions are retained without numerical attenuation. This shall allow the formulation to be readily applied also to sharp transient excitations, such as by Heaviside step input, impulsive action, or impact loading, whose high-frequency content shall play a dominant role in the resulting dynamic response.

### 2.2. Development of the ENTI method for a discretized FEM ML problem

In this section, a ML problem is formulated for a 1D straight beam discretized using Euler-Bernoulli beam FEs, whose resulting dynamic equations of motion are exactly solved with the proposed ENTI method.

The ML is modelled as a concentrated force of constant magnitude $F$ travelling at constant speed $v$ along the beam (for instance from left to right). The instantaneous position of the load is defined in the global reference system by coordinate $x_L(t) = vt$. Conversely, the relative position in the local FE is defined within the local reference system of the active FE, denoted as $e$-th element, and currently supporting the load. The origin of this local reference system is fixed to the first node of this FE, $x_{e1}$; thus, relative FE coordinate $x_r(t)$ is expressed as follows:

$$x_r(t) = x_L(t) - x_{e1} \tag{17}$$

Since the ML traverses the whole beam length, acting at positions also distinct from mesh nodes, its effect is modelled through equivalent nodal forces that vary continuously with time. Furthermore, as the load progresses in the position, the active element and the corresponding DOFs change over time. Consequently, tracking relative position $x_r(t)$ is essential, to correctly assemble global external force vector $\mathbf{F}(t)$. For the $e$-th element, the equivalent nodal forces are obtained from Hermitian shape functions $\psi_i(x)$; thus, element force vector $\mathbf{F}_e(t)$ can be expressed as:

$$\mathbf{F}_e^{\mathrm{T}}\left(x_r(t)\right) = F\left[\psi_1(x_r), \psi_2(x_r), \psi_3(x_r), \psi_4(x_r)\right] \tag{18}$$

where third-order polynomial shape functions $\Psi_i(x_r)$ depend on relative coordinate $x_r$ scaled by FE length $h$:

$$\psi_1(x_r) = 1 - 3\left(\frac{x_r}{h}\right)^2 + 2\left(\frac{x_r}{h}\right)^3 \tag{19a}$$

$$\psi_2(x_r) = x_r - 2h\left(\frac{x_r}{h}\right)^2 + h\left(\frac{x_r}{h}\right)^3 \tag{19b}$$

$$\psi_3(x_r) = 3\left(\frac{x_r}{h}\right)^2 - 2\left(\frac{x_r}{h}\right)^3 \tag{19c}$$

$$\psi_4(x_r) = -h\left(\frac{x_r}{h}\right)^2 + h\left(\frac{x_r}{h}\right)^3 \tag{19d}$$

In Eqs. (19a)–(19d) odd-index functions are associated with nodal displacements, while even-index functions correspond to nodal rotations.

In the global FEM model, only the DOFs belonging to the active beam element exhibit non-zero values of the equivalent nodal forces; thus, global force vector $\mathbf{F}(t)$ is defined as follows:

$$\mathbf{F}^{\mathrm{T}}(t) = \left[\mathbf{0}^{\mathrm{T}}, \ldots, \mathbf{F}_e^{\mathrm{T}}, \ldots, \mathbf{0}^{\mathrm{T}}\right] \tag{20}$$

To apply the ENTI method, state-space force term $\mathbf{T}(t)$ (Eq. (5)) must be evaluated starting from $\mathbf{F}(t)$, as defined in Eq. (20). A crucial observation concerns the form of this term: since the nodal forces are derived from cubic Hermitian shape functions, $\mathbf{T}(t_n + r)$ preserves a third-order polynomial dependence on local variable $r$. As a result, the convolutional integral appearing in Eq. (14) takes the specific form of a product between an exponential matrix and a polynomial vector, resulting particularly advantageous as it admits a closed-form analytical solution. By applying repeated integrations by parts, the integral can be resolved, exactly, into a finite series of terms, thereby avoiding any approximation error associated with numerical quadrature.

In fact, force vector $\mathbf{F}(t_n + r)$, evaluated at time instant $t_n + r$, is expressed as a standard third-order polynomial for $0 \le r \le \Delta t$:

$$\mathbf{F}(t_n + r) = \mathbf{F}_0(t_n) + \mathbf{F}_1(t_n)\left(\frac{r}{\Delta t}\right) + \mathbf{F}_2(t_n)\left(\frac{r}{\Delta t}\right)^2 + \mathbf{F}_3(t_n)\left(\frac{r}{\Delta t}\right)^3 \tag{21}$$

Therein, time-dependent coefficient-vectors $\mathbf{F}_0(t)$, $\mathbf{F}_1(t)$, $\mathbf{F}_2(t)$, $\mathbf{F}_3(t)$ are sparse, containing zero elements for all the DOFs except for those associated with the element currently being traversed by the ML. For the active DOFs, the non-zero entries are derived using the FEM shape functions given in Eqs. (19a)–(19d), evaluated at relative position $x_r(t_n + r) = v \cdot (t_n + r) - x_{e1}$ and magnified with the load amplitude. Specifically, these expressions are obtained by expanding the polynomial functions according to local time increment $r$. By collecting the

terms associated with normalized powers $(r/\Delta t)$, $(r/\Delta t)^2$ and $(r/\Delta t)^3$, local contribution vectors $\mathbf{F}_{1,e}$, $\mathbf{F}_{2,e}$, and $\mathbf{F}_{3,e}$ are identified by expanding the polynomial shape functions as follows:

$$\mathbf{F}_{0,e}(t_n) = \mathbf{F}_e(t_n) \tag{22a}$$

$$\mathbf{F}_{1,e}(t_n) = F x_r \frac{v}{h} \begin{bmatrix} -6/h + 6x_r/h^2 \\ -4 + 3x_r/h + h/x_r \\ 6/h - 6x_r/h^2 \\ -2 + 3x_r/h \end{bmatrix} \Delta t \tag{22b}$$

$$\mathbf{F}_{2,e}(t_n) = F \frac{v^2}{h} \begin{bmatrix} -3/h + 6x_r/h^2 \\ -2 + 3x_r/h \\ 3/h - 6x_r/h^2 \\ -1 + 3x_r/h \end{bmatrix} \Delta t^2 \tag{22c}$$

$$\mathbf{F}_{3,e}(t_n) = F \frac{v^3}{h^2} \begin{bmatrix} 2/h \\ 1 \\ -2/h \\ 1 \end{bmatrix} \Delta t^3 \tag{22d}$$

Subsequently, force vector $\mathbf{T}(t_n + r)$ is expressed in the same form of $\mathbf{F}(t_n + r)$:

$$\mathbf{T}(t_n + r) = \mathbf{T}_0(t_n) + \mathbf{T}_1(t_n)\left(\frac{r}{\Delta t}\right) + \mathbf{T}_2(t_n)\left(\frac{r}{\Delta t}\right)^2 + \mathbf{T}_3(t_n)\left(\frac{r}{\Delta t}\right)^3 \tag{23}$$

Once vector $\mathbf{T}(t_n + r)$ is made explicit in its polynomial form, it can directly be substituted into the convolution integral of Eq. (14). By exploiting the linearity of the integral operator, the integral is decomposed into four distinct contributions of $\mathbf{T}(t_n + r)$, corresponding to powers of $r$. As a result, the recursive update of the state vector of Eq. (14) is provided by the following expression:

$$\mathbf{z}(t_{n+1}) = \mathrm{e}^{-\mathbf{S}\Delta t}\,\mathbf{z}(t_n) + \sum_{k=0}^{3} \mathbf{z}_{p,k}(t_{n+1}) \tag{24}$$

where the first term refers to the homogeneous solution, associated to a free vibration, while the sum of $\mathbf{z}_{p,k}(t_{n+1})$, $k = 0, 1, 2, 3$ constitutes the particular solution. Specifically, each $\mathbf{z}_{p,k}$ term arises from the convolution of the exponential matrix with the $k$-th order polynomial component of the load.

The integration of single terms $\mathbf{z}_{p,k}$ is analytically performed via repeated integration by parts, and a distinct recursive structure emerges from such a derivation. It is observed that the integral of the term associated with order $k + 1$ is strictly dependent on the result of order $k$ and this recursive property may be generalized. By defining coefficient matrices $\mathbf{A}_k$ as the solutions of the convolutional integral, the terms constituting the particular solution are evaluated as follows:

$$\mathbf{z}_{p,0}(t_{n+1}) = \mathbf{A}_0\mathbf{T}_0(t_n) \tag{25a}$$

$$\mathbf{z}_{p,1}(t_{n+1}) = \mathbf{A}_1\mathbf{T}_1(t_n) \tag{25b}$$

$$\mathbf{z}_{p,2}(t_{n+1}) = \mathbf{A}_2\mathbf{T}_2(t_n) \tag{25c}$$

$$\mathbf{z}_{p,3}(t_{n+1}) = \mathbf{A}_3\mathbf{T}_3(t_n) \tag{25d}$$

where resulting coefficient matrices $\mathbf{A}_k$ are determined through the following recursive evaluation, which ensures an exact integration:

$$\mathbf{A}_0 = \mathbf{S}^{-1}\left(\mathbf{I} - \mathrm{e}^{-\mathbf{S}\Delta t}\right) \tag{26a}$$

$$\mathbf{A}_1 = \mathbf{S}^{-1}\left(\mathbf{I} - \frac{\mathbf{A}_0}{\Delta t}\right) \tag{26b}$$

$$\mathbf{A}_2 = \mathbf{S}^{-1}\left(\mathbf{I} - \frac{2\mathbf{A}_1}{\Delta t}\right) \tag{26c}$$

$$\mathbf{A}_3 = \mathbf{S}^{-1}\left(\mathbf{I} - \frac{3\mathbf{A}_2}{\Delta t}\right) \tag{26d}$$

Finally, the displacement, velocity, and acceleration vectors are extracted by the state variables through the extraction matrices, Eq. (15), according to Eqs. (16a)–(16c).

The proposed ENTI method may be contextualized within the framework of so-called "exponential integrators". Both approaches share a common theoretical origin, relying on the exponential matrix, to provide an exact solution to the linear differential equations. Moreover, herein derived recursive coefficients $\mathbf{A}_k$ shall formally be equivalent to scaled variations of so-called standard $\varphi$-functions [28,63,64], largely employed in this class of exponential integrators, specifically detailed in Exponential Time Differencing (ETD) and in exponential Runge-Kutta methods (see Hochbruck and Ostermann 2010 [28]), with $\mathbf{A}_k(-\mathbf{S}\Delta t) = k!\,\Delta t\,\phi_{k+1}(-\mathbf{S}\Delta t)$).

A distinguishing feature of the present ENTI method lies in the treatment of the forcing term. Generally, exponential integrators employ numerical quadrature to handle arbitrary loading functions. Instead, herein the ENTI method takes advantage of the specific polynomial nature of the FEM ML setting, allowing for a closed-form analytical evaluation, via the recursive procedure expressed in Eqs. (26a)–(26d), leading to the elimination of truncation errors associated with numerical quadrature.

Coherently, one shall remark that herein the evaluation of all dynamic response variables, specifically including accelerations, is wholly exact. Like that, convergence studies or demonstrations on convergence rates, as typically characteristic or even necessary for the evaluation of classical numerical integrators, are simply extraneous to the present context.

Furthermore, since time interval $\Delta t$ is herein chosen as constant along the time history, exponential matrix $\mathrm{e}^{-\mathbf{S}\Delta t}$, and $\mathbf{A}_k$ coefficients are computed only at once, during the pre-processing phase. Details on these crucial computational aspects are provided in the following sections.

Notably, the present ENTI method is herein established for Linear Time-Invariant (LTI) systems under Moving Load assumption, where state matrix $\mathbf{S}$ remains constant, allowing exponential matrix $\mathrm{e}^{-\mathbf{S}\Delta t}$ to be evaluated just at once during the initialization phase. For full Vehicle-Structure Interaction problems (e.g., for Moving Mass or Moving Oscillator problems), the time-varying nature of state matrix $\mathbf{S}(t)$ may require alternative approaches for the handling of the dynamic problem; thereby, in order to tackle this issue, alternative numerical strategies may be explored in future endeavours of the present cornerstone developments of the ENTI method.

## 3. Computational implementation of the ENTI method

The ENTI method has been implemented within a MATLAB environment, with particular attention to achieve computational efficiency and numerical robustness of the procedure. A central objective of the implementation was to minimize the number of mathematical operations (sums, multiplications, etc.) executed within the time-stepping loop, thereby reducing the computational cost and most of all limiting the accumulation of pure round-off errors throughout the integration process.

It is worth emphasizing that the computational implementation itself shall constitute a peculiar contribution of this work. By structuring the procedure to pre-compute matrices and vectors that are independent of the time step, the present ENTI implementation allows the main loop to focus exclusively on updating the system state and evaluating the various response variables. This coding ensures both a high efficiency and a robust, reproducible framework, which may be applied to a broad class of discretized structural systems subjected to MLs.

### 3.1. Pre-processing of the ML and evaluation of the required matrices

The first stage of the ENTI procedure consists in pre-processing the time evolution of the ML and assembling all matrices that remain constant during the time-integration process. The force transmitted by the load to the structure is expressed through third-order polynomial shape functions, and its time-dependent contributions are stored in vectors $\mathbf{F}_0(t)$, $\mathbf{F}_1(t)$, $\mathbf{F}_2(t)$, $\mathbf{F}_3(t)$, collected column-wise in a global (dedicated) force matrix. This enables efficient access to the load history during the time-stepping phase.

In the FEM ML problem, a constant time step may be defined as:

$$\Delta t = \frac{h/v}{n_{\text{steps}}} \tag{27}$$

where $h$ is again the FE length, $v$ the travelling speed of the ML, and $n_{\text{steps}}$ the number of steps required for the ML to travel across a single FE. At each time step, a $4 \times 1$ vector is shifted within the global force matrix so that the non-zero load component consistently moves along the beam.

All constant matrices required by the ENTI formulation are assembled in advance. Specifically, state matrix $\mathbf{S}$ in Eq. (5) is computed from system matrices $\mathbf{M}, \mathbf{C}, \mathbf{K}$, and is readily complemented by its inverse, $\mathbf{S}^{-1}$, which can be obtained via block inversion (assuming $\mathbf{K}$ to be invertible), as follows:

$$\mathbf{S}^{-1} = \begin{bmatrix} \mathbf{K}^{-1}\mathbf{C} & \mathbf{K}^{-1}\mathbf{M} \\ -\mathbf{I} & \mathbf{0} \end{bmatrix} \tag{28}$$

This closed-form block expression is numerically advantageous, since it avoids the direct inversion of full matrix $\mathbf{S}$, whose lower blocks are dense. The computation requires only matrices $\mathbf{K}^{-1}\mathbf{C}$ and $\mathbf{K}^{-1}\mathbf{M}$ to be formed, and in the undamped case only the latter. Notice that the evaluation of $\mathbf{S}$ requires the computation of $\mathbf{M}^{-1}$; the evaluation of $\mathbf{S}^{-1}$, needs the computation of $\mathbf{K}^{-1}$. This condition may not be fulfilled when unconstrained structures, floating bodies, or systems with rigid-body modes may be included in the structural model. This makes singular stiffness matrix $\mathbf{K}$, and state matrix $\mathbf{S}$, and to handle the singularity of these matrices, the formulation may be extended via modal decomposition. Specifically, for the homogeneous solution, exponential matrix $e^{-\mathbf{S}\Delta t}$ inherently handles zero-frequency eigenvalues without requiring any matrix inversion, thereby capturing rigid-body motions exactly as is. For the particular solution, decoupling the equations of motion in the modal space allows for the splitting of the zero-frequency rigid-body modes and the non zero-frequency deformable modes; then, time integration can be performed separately and directly in the time domain, completely bypassing the singularity of $\mathbf{S}$. However, a detailed discussion about that shall be specialized to specific cases and may be reported elsewhere, when needed.

Also, exponential matrix $e^{-\mathbf{S}\Delta t}$ is evaluated in the pre-processing phase to avoid repeated computations within the loop over the time steps. In the literature, the exponential matrix is typically computed through various numerical schemes. Specifically, the MATLAB environment provides built-in function `expm`, which implements a scaling-and-squaring algorithm combined with a Padé approximation [61,62]. However, for the LTI system under consideration, an analytical closed-form expression for the exponential matrix may be obtained, and adopted, according to the specific damping modelling assumptions (classical or Rayleigh damping), as derived below.

### 3.1.1. No-damping model

When the model is assumed to be undamped, namely $\mathbf{C} = \mathbf{0}$, a closed-form computation of $e^{-\mathbf{S}\Delta t}$ may be carried out through the following expression in the eigenvector basis of matrices $\mathbf{M}$ and $\mathbf{K}$:

$$e^{-\mathbf{S}\Delta t} = \begin{bmatrix} \mathbf{\Phi} & \mathbf{0} \\ \mathbf{0} & \mathbf{\Phi} \end{bmatrix} \begin{bmatrix} \mathbf{G}_{11}(\Delta t) & \mathbf{G}_{12}(\Delta t) \\ \mathbf{G}_{21}(\Delta t) & \mathbf{G}_{22}(\Delta t) \end{bmatrix} \begin{bmatrix} \mathbf{\Phi}^{\mathrm{T}}\mathbf{M} & \mathbf{0} \\ \mathbf{0} & \mathbf{\Phi}^{\mathrm{T}}\mathbf{M} \end{bmatrix} \tag{29}$$

where matrix $\mathbf{\Phi}$ is the system eigenvector matrix (normalized as $\mathbf{\Phi}^{\mathrm{T}}\mathbf{M}\mathbf{\Phi} = \mathbf{I}$, which is associated to diagonal eigenvalue matrix $\mathbf{\Phi}^{\mathrm{T}}\mathbf{K}\mathbf{\Phi} = \mathbf{\Omega}^2$) containing the column eigenvectors of the structural system, and $\mathbf{G}_{ij}$ are the modal time-evolution matrix functions, which can be defined as:

$$\mathbf{G}_{11}(\Delta t) = \cos(\mathbf{\Omega}\Delta t) \tag{30a}$$

$$\mathbf{G}_{12}(\Delta t) = \mathbf{\Omega}^{-1}\sin(\mathbf{\Omega}\Delta t) \tag{30b}$$

$$\mathbf{G}_{21}(\Delta t) = \dot{\mathbf{G}}_{11}(\Delta t) = -\mathbf{\Omega}\sin(\mathbf{\Omega}\Delta t) \tag{30c}$$

$$\mathbf{G}_{22}(\Delta t) = \dot{\mathbf{G}}_{12}(\Delta t) = \cos(\mathbf{\Omega}\Delta t) = \mathbf{G}_{11}(\Delta t) \tag{30d}$$

In this setting, the evaluation of the trigonometric matrix functions is straightforward, since the cosine or sine of a diagonal matrix are obtained by applying the corresponding scalar function to each diagonal entry. As a result, the cosine and sine matrices reduce to simple diagonal element-wise operations.

The derivation of this expression, reported in Appendix A, begins with the homogeneous solution of the second-order system of ODEs, in principal coordinates (see Eq. (36), in Appendix A; a representation similar to Eqs. (29), (30) has been provided in [37]). The resulting displacement and velocity vectors are assembled into a state-space representation and transformed back into the physical domain. By comparing this assembled solution with that obtained from the state-space representation (Eq. (6)) involving the exponential matrix of $-\mathbf{S}\Delta t$, the explicit block-partitioned form of the exponential matrix is identified. All detailed steps of this analytical procedure are provided in Appendix A.

Conversely, MATLAB function `expm`, which may commonly be used to numerically compute the exponential matrix, is as well tested, in the context of the dynamic simulations, against the exact analytical expressions in Eqs. (29), (30), to quantify the error that may be introduced by the numerical evaluation of the exponential matrix.

To this end, a sensitivity analysis is proposed across different time steps. According to the structural properties defined in following Section 4, for the structural problem at hand, matrix $\mathbf{S}$ assumes dimensions $1010 \times 1010$ and time interval $\Delta t$ is calculated based on the number of steps $n_{steps}$ required for the load to travel across a single FE. Then, $n_{steps}$ ranges from 10 to 100,000, corresponding to time step size $\Delta t$ ranging from around $10^{-3}$ to $10^{-7}$ s.

In particular, two error metrics are adopted for comparison purposes: absolute error and relative error, both computed starting from the absolute differences between the exponential matrices and the latter scaled by the maximum value registered by the reference analytical matrix. A representation in double logarithmic scale of the recorded errors for the undamped case is provided in Fig. 1.

By varying $\Delta t$ by powers of 10, both absolute and relative errors decrease with two main distinct slopes in log-log scale. This reduction is attributed to the decrease in the time interval, leading to a subsequent diminution in the required number of scaling-and-squaring operations in the Padé approximation adopted by `expm`. Consequently, global truncation and round-off errors decrease, due to their reduced accumulation during matrix power iterations.

Focusing on the trend of the relative error, weighted by the maximum entry of the exponential matrix, the observed reduction in Fig. 1

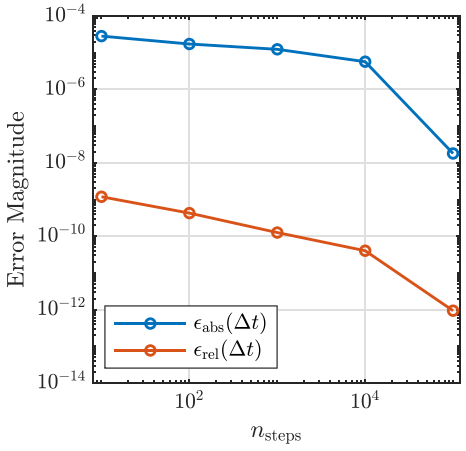



**Fig. 1.** Maximum absolute error $\epsilon_{\text{abs}}(\Delta t) = \max|\mathbf{E}_{\text{expm}} - \mathbf{E}_{\text{exact}}|$ and relative error $\epsilon_{\text{rel}}(\Delta t) = \epsilon_{\text{abs}}/\max|\mathbf{E}_{\text{exact}}|$ (dimensionless) between exponential matrix computed using MATLAB's `expm` and given closed-form expression (undamped system configuration), in double logarithmic scale.

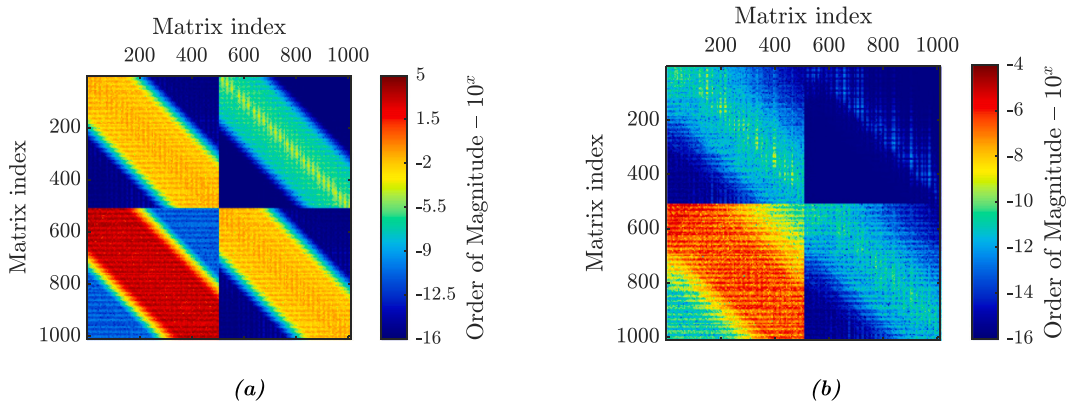



**Fig. 2.** Analysis of exponential matrix $e^{-\mathbf{S}\Delta t}$ evaluation for the undamped configuration: (a) order of magnitude of the analytical entries and (b) spatial distribution of the absolute numerical error with respect to `expm`, for $n_{\text{steps}} = 100$.

is almost linear in log-log scale up to $10^4$ steps, where a significant subsequent drop in the error is then noticed. However, for number of steps on the EF, in the range between 10 to 1000, the relative difference is in the order of magnitude of $10^{-10}$-$10^{-9}$.

To provide a better understanding of the error introduced by `expm` in the evaluation of exponential matrix $e^{-\mathbf{S}\Delta t}$, Fig. 2 further represents a distribution of the magnitudes of the analytical exponential matrix entries and the difference with those numerically computed for a time interval of $n_{steps} = 100$.

In particular, this analysis reveals that largest errors appear in South-West block (2,1) of the exponential matrix (stiffness related terms), where the absolute error in red is in the order of $10^{-7}$-$10^{-6}$, while the value of the entries in the other blocks is about $10^3$-$10^4$, leading to a maximum relative error of approximately $4.27 \cdot 10^{-10}$. Instead, in other blocks, the relative error reaches a lower value of around $10^{-11}$-$10^{-12}$.

These results suggest that the adoption of the closed-form expression of the exponential matrix shall offer significant advantages, in terms of long-term numerical accuracy. By eliminating external sources of evaluation error at each step, the ENTI method shall remain robust even over a great number of time increments.

In contrast, only for shorter simulations, the cumulative error introduced by numerical schemes, such as MATLAB's `expm`, may remain within acceptable limits, due to the limited number of steps. Furthermore, due to the inherent characteristics of exponential integrators, the time step could be chosen to be much larger than in common numerical integration schemes; consequently, this reduction in the total number of steps may mitigate the amount of cumulative errors, although the analytical closed-form evaluation remains the only approach that shall ensure theoretical exactness, regardless of simulation's duration.

### 3.1.2. Classical damping model

In structural dynamics, damping is frequently modelled using a classical damping assumption. This approach hypothesizes that damping matrix $\mathbf{C}$ may be diagonalized in the same undamped eigenvector basis, via same modal matrix $\mathbf{\Phi}$, consistently with the aforementioned normalization ($\mathbf{\Phi}^{\mathrm{T}}\mathbf{M}\mathbf{\Phi} = \mathbf{I}$), and eigenvalue matrix $\mathbf{\Omega}^2 = \mathbf{\Phi}^{\mathrm{T}}\mathbf{K}\mathbf{\Phi}$, coming from mass $\mathbf{M}$ and stiffness $\mathbf{K}$ matrices:

$$\mathbf{\Phi}^{\mathrm{T}}\mathbf{C}\mathbf{\Phi} = 2\mathbf{Z}\mathbf{\Omega} \tag{31}$$

where $\mathbf{Z}$ is a diagonal matrix that collects given modal damping ratios $\zeta_i$.

Analogously to the undamped system, the exponential matrix of $-\mathbf{S}\Delta t$ is calculated with the same structure in Eq. (29). Assuming an inherent subcritical damping regime ($0 \le \zeta_i < 1,\ \forall i$), the corresponding modal time-evolution matrix functions are computed as:

$$\mathbf{G}_{11}(\Delta t) = e^{-\mathbf{Z}\mathbf{\Omega}\Delta t}\left[\cos(\mathbf{\Omega}_d\Delta t) + \mathbf{Z}\mathbf{\Omega}\mathbf{\Omega}_d^{-1}\sin(\mathbf{\Omega}_d\Delta t)\right] \tag{32a}$$

$$\mathbf{G}_{12}(\Delta t) = e^{-\mathbf{Z}\mathbf{\Omega}\Delta t}\mathbf{\Omega}_d^{-1}\sin(\mathbf{\Omega}_d\Delta t) \tag{32b}$$

$$\mathbf{G}_{21}(\Delta t) = \dot{\mathbf{G}}_{11}(\Delta t) = -e^{-\mathbf{Z}\mathbf{\Omega}\Delta t}\mathbf{\Omega}^2\mathbf{\Omega}_d^{-1}\sin(\mathbf{\Omega}_d\Delta t) \tag{32c}$$

$$\mathbf{G}_{22}(\Delta t) = \dot{\mathbf{G}}_{12}(\Delta t) = e^{-\mathbf{Z}\mathbf{\Omega}\Delta t}\left[\cos(\mathbf{\Omega}_d\Delta t) - \mathbf{Z}\mathbf{\Omega}\mathbf{\Omega}_d^{-1}\sin(\mathbf{\Omega}_d\Delta t)\right] \tag{32d}$$

where $\mathbf{\Omega}_d = \mathbf{\Omega}\sqrt{\mathbf{I} - \mathbf{Z}^2}$ corresponds to the diagonal matrix of damped natural frequencies. The derivation of these modal time-evolution matrix functions is similar to that outlined for the undamped system. Obviously, for the undamped case ($\mathbf{Z} = \mathbf{0}$) the expressions in Eqs. (32) reduce to those in Eqs. (30). The details about the derivation may additionally be found in Appendix B.

As for the undamped system, an analogous sensitivity analysis may be conducted with the same mass and stiffness matrices for the damped system, while randomly assigning classical modal damping ratios $\zeta_i$ in the light subcritical range from 0 to 10%, in descending order. This analysis aims to assess the influence of structural damping on the numerical evaluation of the exponential matrix. The results are reported in Fig. 3, where the absolute error slightly increases from the order of $10^{-6}$ to $10^{-5}$, at $10^3$ steps per FE, before showing a sharp drop to $10^{-8}$. Conversely, the relative error displays an almost linear decrease in logarithmic scale starting from $10^{-9}$ to $10^{-10}$ for $n_{steps} = 10,\ 100$, then remains constant at $10^{-10}$ up to $n_{steps} = 1000$, subsequently showing a sharp decrease to $10^{-12}$. The observed slope of approximately $-1$ in log-log scale indicates that the relative error is about inversely proportional to the number of steps (i.e., a tenfold increase in steps results in a tenfold reduction of the error), as $\Delta t$ linearly decreases as the number of steps increases. Consequently, the numerical evaluation of the exponential matrix via `expm` becomes significantly more accurate as $\Delta t$ approaches zero, explaining the observed trend.

Regarding numerical accuracy, the maximum relative error recorded is $7.00 \cdot 10^{-10}$ and is strictly comparable to that observed in the undamped configuration ($1.19 \cdot 10^{-9}$), indicating that the inclusion of dissipative terms does not significantly alter the algorithmic precision. The maximum absolute error is found to be in the order of $10^{-6}$, more precisely $9.25 \cdot 10^{-6}$, specifically located in South-West sub-block (2,1) (stiffness-related terms), as represented in Fig. 4(b), where the matrix entries reach magnitudes of approximately $10^3$ along the diagonal. Conversely, in the other blocks, the relative error drops down to the order of $10^{-10}$-$10^{-12}$.

In conclusion, these results show that for both undamped and classically damped systems, the closed-form evaluation of the exponential matrix may considerably reduce the cumulative error effect in the solution, for long simulations, of about $10^6$ or more time steps, as the analytical exponential matrix shall not introduce numerical errors.

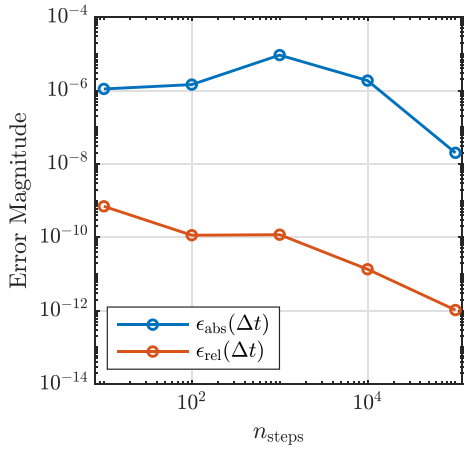



**Fig. 3.** Maximum absolute error $\epsilon_{abs}(\Delta t) = \max |\mathbf{E}_{expm} - \mathbf{E}_{exact}|$ and relative error $\epsilon_{rel}(\Delta t) = \epsilon_{abs} / \max |\mathbf{E}_{exact}|$ (dimensionless) between exponential matrix computed using MATLAB's `expm` and given closed-form expression (damped system configuration), in double logarithmic scale.

However, for shorter simulations, the cumulative error introduced by the numerically calculated exponential matrix may remain bounded. In such a case, employing a coarser time discretization (larger $\Delta t$) may introduce a higher numerical residual in the evaluation of the exponential matrix; on the other hand, it may reduce the total number of recursive operations required for the simulation. Consequently, a trade-off may be achieved by accepting a slightly larger local error, in exchange for a reduction in the overall cumulative error. This feature may appear particularly advantageous for adaptive time-stepping strategies, allowing for the use of refined steps only where necessary, without compromising the global accuracy of the numerical solution, once the exponential matrix is numerically evaluated.

### 3.2. Optimized ENTI implementation

The ENTI algorithm is structured to pre-compute all matrices and vectors that are independent of the (constant) time step, leaving the main loop to solely operate on updating state vector $\mathbf{z}$ and computing response variables $\mathbf{u}$, $\dot{\mathbf{u}}$, and $\ddot{\mathbf{u}}$.

This pre-processing phase involves evaluating block matrices $\mathbf{S}$ and $\mathbf{S}^{-1}$ (Eqs. (5) and (28)), and force history vectors $\mathbf{F}_0, \mathbf{F}_1, \mathbf{F}_2, \mathbf{F}_3$ (Eqs. (22b)–(22d)), along with corresponding term vectors $\mathbf{T}_0, \mathbf{T}_1, \mathbf{T}_2, \mathbf{T}_3$ (Eq. (5)). Specifically, exponential matrix $e^{-\mathbf{S}\Delta t}$ is herein determined by using the proposed closed-form analytical expression (Eq. (29)); however, it could alternatively be numerically computed using MATLAB built-in function `expm` (see discussion in the previous subsections).

**Algorithm 1** Pseudo–code ENTI strategy for ML problems – optimized implementation.

*Pre-processing phase*
Compute dynamic system matrices: $\mathbf{M}$, $\mathbf{C}$, $\mathbf{K}$
Set constant time step $\Delta t$
Compute force vector $\mathbf{F}(t)$
Compute state-space matrices $\mathbf{S}$, $\mathbf{S}^{-1}$, and exponential matrix $e^{-\mathbf{S}\Delta t}$ (exactly)
Compute matrices $\mathbf{A}_0$, $\mathbf{A}_1$, $\mathbf{A}_2$, $\mathbf{A}_3$
Compute known force coefficients $\mathbf{F}_0$, $\mathbf{F}_1$, $\mathbf{F}_2$, $\mathbf{F}_3$
Compute vectors $\mathbf{T}_0$, $\mathbf{T}_1$, $\mathbf{T}_2$, $\mathbf{T}_3$
Initialize state variables: $\mathbf{z} = [\mathbf{z}^{(0)}, \mathbf{0}, \dots, \mathbf{0}]$

*Forced vibration phase ($n = 0$ to $n_{exit} - 1$)*
**for** $n = 0$ to $n_{\text{exit}} - 1$ **do**
    Compute and store next state:
    $\mathbf{z}(:, n+1) \leftarrow e^{-\mathbf{S}\Delta t}\mathbf{z}(:, n) + \mathbf{A}_0\mathbf{T}_0^{(n)} + \mathbf{A}_1\mathbf{T}_1^{(n)} + \mathbf{A}_2\mathbf{T}_2^{(n)} + \mathbf{A}_3\mathbf{T}_3^{(n)}$
**end for**

*Free vibration phase ($n = n_{exit}$ to $n_{time} - 1$)*
**for** $n = n_{\text{exit}}$ to $n_{\text{time}} - 1$ **do**
    $\mathbf{z}(:, n+1) \leftarrow e^{-\mathbf{S}\Delta t}\mathbf{z}(:, n)$
**end for**

*Post-processing: matrix-form extraction of kinematic quantities*
Extract nodal displacements
$\mathbf{u} \leftarrow \mathbf{L}_1\mathbf{z}$
Extract nodal velocities
$\dot{\mathbf{u}} \leftarrow \mathbf{L}_2\mathbf{z}$
Extract nodal accelerations
$\ddot{\mathbf{u}} \leftarrow \mathbf{L}_2\dot{\mathbf{z}}$

The core of the method is the time-stepping loop, where state vector $\mathbf{z}$ is updated by summing up the four contributions in Eq. (24), where $\mathbf{z}_{p,k}(t_n)$ is herein denoted as $\mathbf{z}_{p,k}^n$, with $n$ the current index of time, and $\mathbf{T}_k(t_n)$ with $\mathbf{T}_k^n$:

$$\mathbf{z}_{p,0}^{n+1} = A_0\mathbf{T}_0^n, \quad \mathbf{z}_{p,1}^{n+1} = A_1\mathbf{T}_1^n, \quad \mathbf{z}_{p,2}^{n+1} = A_2\mathbf{T}_2^n, \quad \mathbf{z}_{p,3}^{n+1} = A_3\mathbf{T}_3^n \tag{33}$$

where $\mathbf{T}_0^{(n)} = \mathbf{T}(t_n)$. Finally, the acceleration vector is evaluated from the state-space representation in Eq. (16c).

Once the ML exits the structure, the simulation enters a subsequent *free vibration phase*, in which the state vector is propagated solely through multiplication by the exponential matrix.

This optimized implementation, pseudo-coded in Algorithm 1, ensures computational efficiency, by restricting the costly operations to the pre-processing stage, while maintaining an exact integration of the

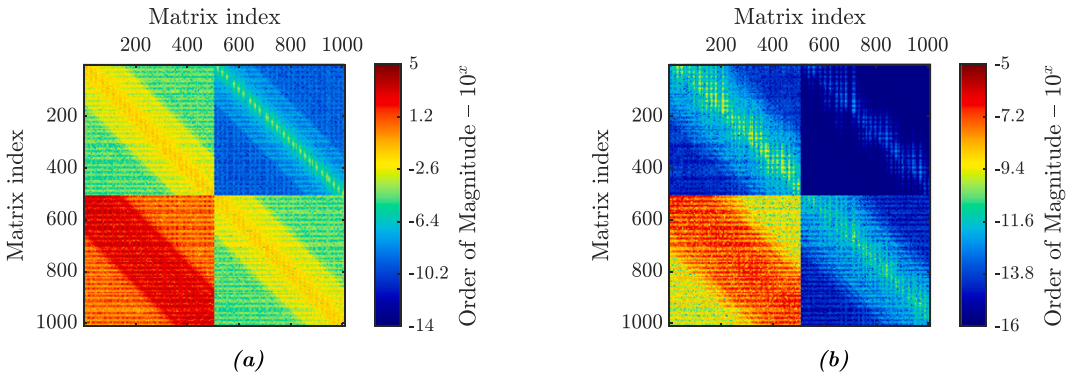



**Fig. 4.** Analysis of exponential matrix $e^{-\mathbf{S}\Delta t}$ evaluation for the damped configuration: (a) order of magnitude of the analytical entries and (b) spatial distribution of the absolute numerical error with respect to `expm`, for $n_{steps} = 100$.

equations of motion. The design is fully general, allowing for the application to undamped or lightly damped systems, and may be extended to more complex polynomial representations of the ML or other forcing functions.

### 3.3. Salient issues on ENTI formulation and implementation

Based on the aforementioned ENTI formulation and implementation, the following salient remarks shall be considered. Specifically, the issues refer to various technical aspects of the implementation, which aims to develop an efficient algorithm and, most importantly, to provide an "exact" solution. While the method is analytically exact and should not introduce any approximation in the time-integration process, its implementation in a MATLAB environment may lead to errors in the order of "machine precision", herein referring to standard double-precision arithmetics (with a limit of approximately $10^{-16}$). Consequently, this small error is purely due to computer rounding, and not to the integration scheme itself. Remarks are presented in itemized form:

- *Reduction of the number of operations within the integration loop*. The loop, over all time steps, devoted to the evaluation of the dynamic response, obviously represents the bottleneck of time-integration algorithms in terms of computational burden. Consequently, a possible strategy to optimize the performance of the present ENTI algorithm for FEM models characterized by a relatively limited number of DOFs may consist in reducing the number of operations within each step of the loop and performing in separate previous computations the evaluation of constant matrices $\mathbf{A}_i$ and $\mathbf{S}$, as well as the time evolution of the coefficients of external force vector $\mathbf{T}_i$, stored in matrix form.
- *Pattern recognition for coefficients* $\mathbf{A}_i$. In order to reduce the number of matrix operations, the evaluation of constant coefficients $\mathbf{A}_i$ takes advantage of the recursive pattern reported in Eqs. (26a)–(26d). This drastically reduces the number of operations, since each coefficient is evaluated according to previously evaluated matrices.
- *Matrix inversion of* $\mathbf{S}$. The inverse of matrix $\mathbf{S}$ is utilized to evaluate each coefficient $\mathbf{A}_i$. To avoid the inversion of the overall matrix, a closed-form expression is identified. However, this expression requires the inversion of the stiffness matrix, which is numerically computed within the adopted MATLAB environment. Consequently, this strategy shall be more precise than that directly involving the inversion of matrix $\mathbf{S}$, since this process includes only the inversion of a matrix characterized by half the dimensions of $\mathbf{S}$.
- *Choice of* $\Delta t$. Importantly, in the ENTI method, the inherent accuracy of the dynamic response does not depend on the size of time interval $\Delta t$, as the solution is always exact and independent of the duration of the time step. Actually, the time interval shall be chosen in terms of desired sampling, according to the selected number of evaluations useful to properly investigate the solution locally. In contrast, the selection of a confined time interval is really crucial for the numerical schemes, as their accuracy strictly relates to $\Delta t$; thus, their results become more accurate with shorter time intervals.
- *Adoption of a closed-form exponential matrix*. The linearity of the dynamic equations of motion expressed by a second-order ODEs system leverages the evaluation of the state-transition matrix, in the first-order ODEs representation, and the related exponential matrix, in closed-form, for undamped or classically damped systems. This powerful expression is particularly advantageous as no approximations shall be introduced in the evaluation process. As a result, the exponential matrix is "exact", thus avoiding any source of spurious numerical error that accumulates over time. Otherwise, the exponential matrix may numerically be evaluated by the `expm` function, at the prize of some (confined) numerical error, see the analyses reported in Sections 3.1.1 and 3.1.2.
- *Computational complexity and model scaling*. Evaluating exact exponential matrix $e^{-\mathbf{S}\Delta t}$ via spectral decomposition introduces an initial, one-time computational cost. To assess the numerical scalability of this phase, benchmark tests were performed comparing the proposed exact exponential matrix formulation against MATLAB's built-in `expm` function. The discretization of the continuous beam model, with properties analyzed in the following section, was varied to cover system dimensions $2n$ (size of matrix $\mathbf{S}$) ranging from 1000 to 10000 (corresponding to 500 to 5000 structural DOFs). All numerical benchmarks were executed in MATLAB R2025b on a MacBook Air equipped with an Apple M3 processor and 24 GB of unified memory. As depicted in Fig. 5, fitting a power-law curve $T(n) = c \cdot n^a$ to the execution times reveals that MATLAB's `expm` function scales with an exponent $a \simeq 2.96$, approaching a cubic scaling ($a \simeq 3$) for higher dimensions. In contrast, the proposed exact spectral decomposition strategy exhibits a lower computational scaling, characterized by an exponent $a \simeq 2.35$. This demonstrates a significantly higher efficiency for models up to $10^4$ DOFs, where the initialization cost is paid only once prior to the integration loop. It shall be noted that by adopting the numerical approach for the evaluation of the exponential matrix, relying on the `expm` Matlab function, the results remain accurate, as the approximated state transition matrix still preservers numerical accuracy. Furthermore, for extremely large-scale models ($10^5$+ DOFs), eigensolvers may encounter RAM saturation limits; in such scenarios, model-order reduction strategies may represent possible extensions for the ENTI framework.

## 4. Numerical simulations of the 1D upper continuous beam of historic San Michele Bridge (1889)

The representative case study chosen for applying the proposed ENTI method, which actually motivated its development, is a one-dimensional FEM model of the upper continuous beam of the historic San Michele Bridge (1889), a remarkable iron arch bridge located in Lombardia, northern Italy, spanning the Adda River and connecting the provinces of Lecco (Paderno d'Adda) and Bergamo (Calusco d'Adda) [65].

The upper deck of the viaduct is specifically idealized as a uniform Euler–Bernoulli beam with a total length of 266 m, consisting of eight equal spans of 33.25 m, supported by nine firm bearings. The mechanical and geometric properties of the beam as modelled in the FEM representation are summarized in Table 1 [13,67].

Each span is discretized into 32 standard Euler-Bernoulli FEs, resulting in 256 elements of equal length $h = 1.0390625$ m. The FEM formulation considers vertical displacements and rotations at each node, resulting in 505 free DOFs and 9 constrained displacement DOFs at the beam supports.

For the ML dynamic analysis, several simplifying assumptions are adopted: (i) the self-weight of the beam is neglected; (ii) the structure is assumed to be initially at rest before the load enters the beam; (iii) material damping, expected to be small [66], is neglected, to clearly highlight potential differences among various subsequently considered time-integration schemes. Further details on the structural model and its calibration are reported in [11–13]. This structural model relies on a continuous beam FEM formulation previously published and validated by Froio et al. (2018) [11]. While in the original reference, 34 FEs per span were employed, a discretization of 32 FEs per span is adopted in this study to achieve a more convenient node distribution for structural symmetry, without sacrificing numerical accuracy.

The dynamic response of the 1D FEM model under a ML is evaluated using the proposed ENTI method and compared against classical numerical time-integration schemes, namely the Newmark method [18], the HHT-$\alpha$ method [21], the Wilson-$\theta$ method [19], and the Bathe method [24]. The results obtained from the different numerical schemes

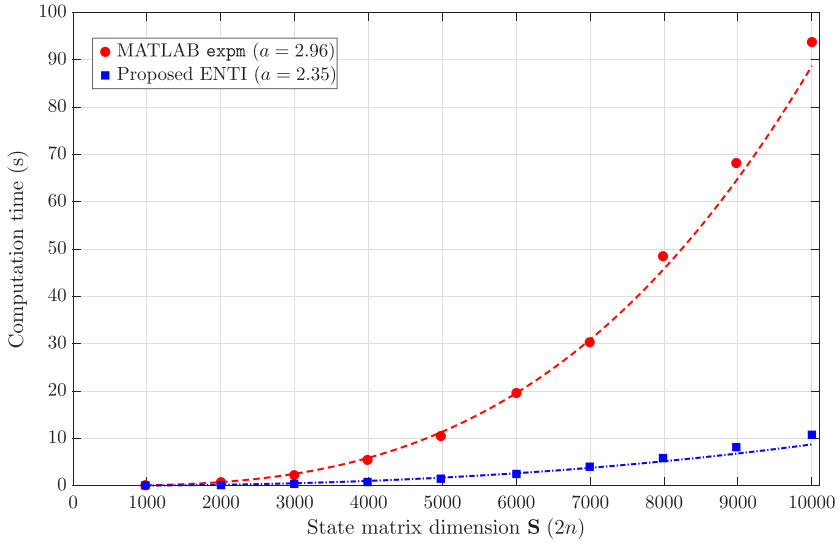



**Fig. 5.** Computational cost comparison between MATLAB's `expm` function and proposed closed-form exponential matrix formulation for matrices of dimensions $2n$ up to 10,000. Red and blue markers denote the measured computation times for the numerical and the closed-form approach matrices, respectively, whereas dashed lines represent corresponding power-law regression curves.

**Table 1**
Mechanical and geometric properties of the multi-supported 1D FEM model of the upper continuous beam of San Michele Bridge (1889).

| | |
|---|---|
| Young's modulus ($E$) | 167 GPa |
| Cross-sectional area ($A$) | $8573 \times 10^{-4}$ m$^2$ |
| Area moment of inertia ($I$) | $9529 \times 10^{-4}$ m$^4$ |
| Mass per unit length ($\mu$) | 6602 kg/m |

are compared in both spatial and temporal domains, as described in following Sections 4.1 and 4.2, respectively, with particular emphasis on the influence of the time-step size. The ML travels along the beam from left to right at a constant velocity of $v = 12.5$ m/s = 45 km/h (as considered in original try-outs in 1889, [68]). Its magnitude is constant, $F = 8.14 \cdot 10^5$ N, corresponding to the gravitational force of a test rail vehicle specifically employed for a recently conducted experimental campaign on the bridge, aimed at characterizing its dynamic response for SHM purposes [69,70].

The solution is investigated for all three dynamic response variables, namely displacements $\mathbf{u}$, velocities $\dot{\mathbf{u}}$, and accelerations $\ddot{\mathbf{u}}$, in terms of deformed configurations and time domain nodal responses. Three different time-step sizes are considered: $\Delta t = 8.3125 \cdot 10^{-3}$ s, $\Delta t = 8.3125 \cdot 10^{-4}$ s, and $\Delta t = 8.3125 \cdot 10^{-5}$ s, corresponding to $n_{steps} = 10$, 100, and 1000 integration steps, respectively, for the ML to traverse a single FE of length $h = 1.0390625$ m.

The simulation comprises a *forced vibration phase* induced by the ML traversing the whole continuous beam and a subsequent *free vibration phase* occurring once the ML exits the structure. The free vibration interval duration equals the time required for the ML to run over a single span.

For the classical time-integration schemes, the adopted parameters are specified as follows: (i) Newmark method with constants $\gamma = 1/2$ and $\beta = 1/4$ (corresponding to the average acceleration formulation); (ii) HHT-$\alpha$ method with $\alpha = (1 - \rho_\infty)/(1 + \rho_\infty) = 0.0256$, determined from an imposed asymptotic spectral radius $\rho_\infty = 0.95$, which allows for a reduced numerical energy dissipation; (iii) Wilson-$\theta$ method with $\theta = 1.4$; (iv) Bathe method with $\gamma = 2 - \sqrt{2}$.

### 4.1. Comparison of space-domain responses (deformed configurations)

Assuming $n_{steps} = 10$ integration steps per FE, the deformed configuration is evaluated with the Moving Load positioned at the midpoint of each span.

Figs. 6 and 7 demonstrate that, for displacements, the numerical schemes provide closely consistent deformation patterns. Table 2 summarizes the maximum displacement values for each span, indicating that deviations among the methods remain within tenths or hundredths of a millimetre, demonstrating the close correspondence among the numerical estimates.

Increasing the number of time steps per FE to 100 and 1000 leads to even progressively smaller discrepancies, with nearly identical results among the methods (Tables 3 and 4). Small amplitude and phase deviations are observed, particularly for the Wilson-$\theta$ method at coarse time steps, but diminishing with refinement.

The deformed configuration corresponding to the global maximum displacement occurs when the load is located 15.07 m from the left end of the first span, and is shown in Fig. 8(a). For this load position, the maximum displacement is 2.768 mm. In Fig. 8(b), a magnified view of the deformation pattern in the region where the displacement field is less pronounced highlights small discrepancies among the numerical schemes, primarily associated with amplitude and phase errors. In particular, the Wilson–$\theta$ method (blue curve) exhibits slightly reduced amplitudes and shifted local maxima, whereas the remaining schemes tend to marginally overestimate the displacement profile.

Similarly to displacements, the velocity and acceleration fields are represented when the maximum value occurs. For the velocity in Fig. 9, this configuration is observed when the load takes its very first initial steps on the beam, namely at $x = 0.73$ m from the left end. In Fig. 9(b), a magnification is provided on the spans far from the load, and it may be observed that only the solution evaluated by the ENTI method experiences the effects of the load arrival in that region.

The acceleration response field registering its maximum value occurs at $t = 22.20$ s (Fig. 10), corresponding to the free-vibration phase. In this scenario, the differences among the methods are much amplified, since accelerations during the free vibration phase seem the most sensitive response variables to modal frequencies. As shown in Fig. 10(b), the field exhibits pronounced high-frequency content, leading to a highly fragmented profile. Consequently, numerical time-integration schemes

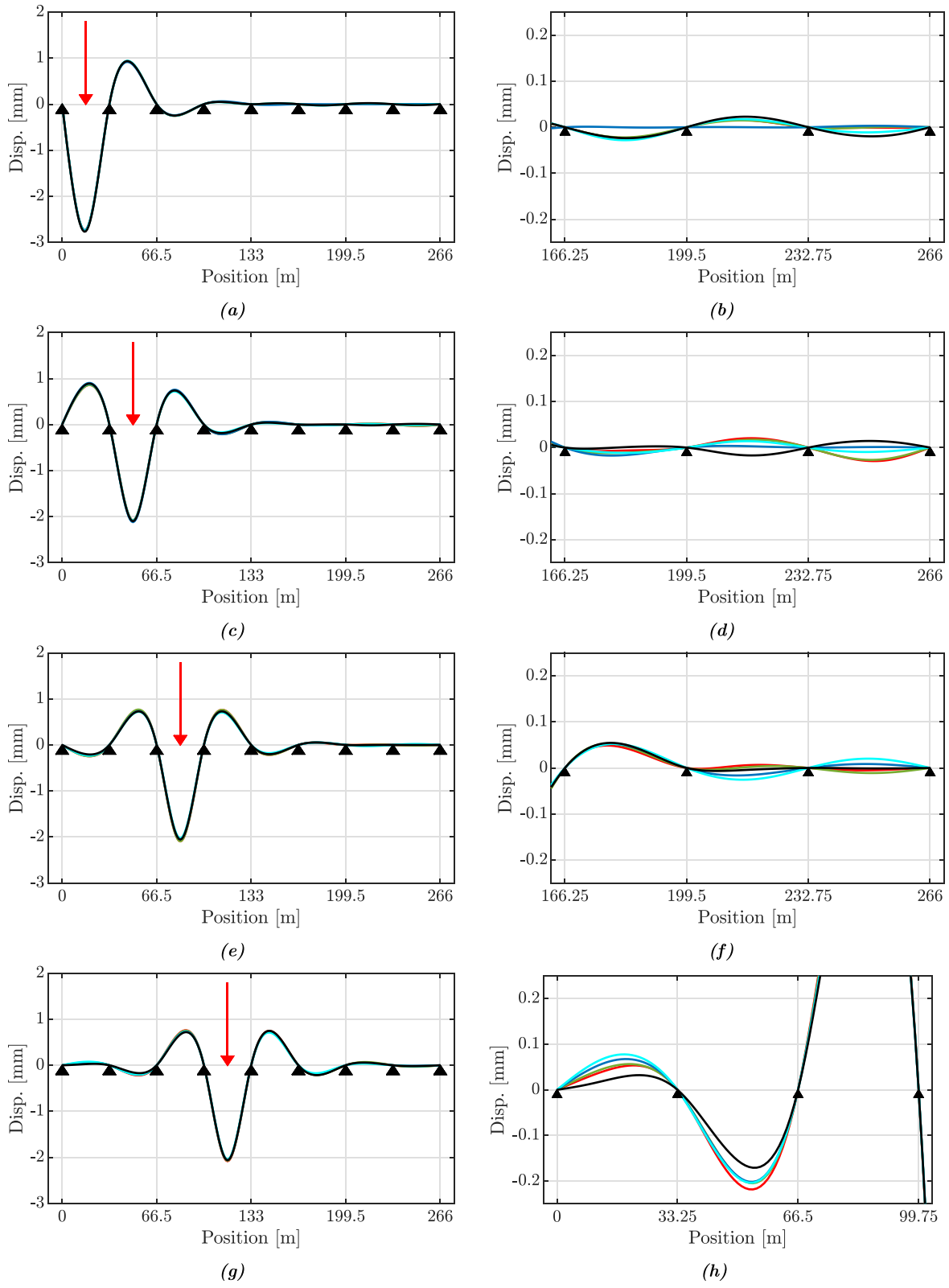



**Fig. 6.** Deformed configuration (displacements) corresponding to ML positioned at the midpoint of the first to fourth spans (red arrow), obtained using the ENTI method (black) and classical time–integration schemes: Newmark (red), HHT-$\alpha$ (green), Wilson-$\theta$ (blue), and Bathe (cyan) (plots (a,c,e,g)). Enlarged view of the sixth to eighth span (plots *b,d,f*) and of the first to third span (plot (h)) highlighting local differences among the numerical solutions. Results refer to 10 time steps per FE.

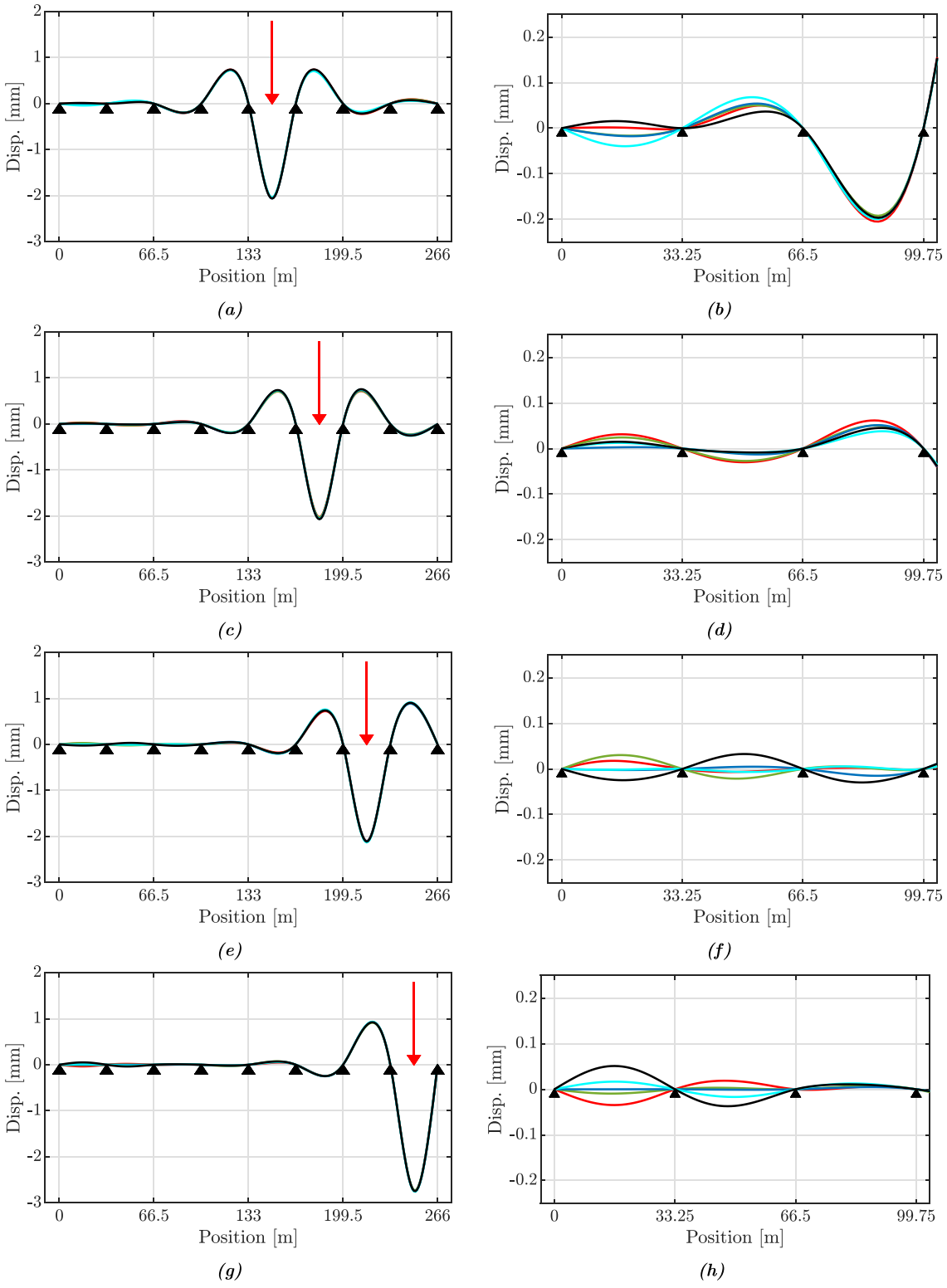



**Fig. 7.** Deformed configuration (displacements) corresponding to the ML positioned at the midpoint of the fifth to eighth spans (red arrow), obtained using the ENTI method (black) and the classical time–integration schemes: Newmark (red), HHT-$\alpha$ (green), Wilson-$\theta$ (blue), and Bathe (cyan) (plots (a,c,e,g)). Enlarged view of the first to third span (plots (b,d,f,h)) highlighting the local differences among the numerical solutions. Results refer to 10 time steps per FE.

**Table 2**
Maximum displacement values at midspan for each span [mm], as computed by the various numerical time–integration methods using 10 time steps per FE.

| Load position | ENTI | Newmark | HHT-$\alpha$ | Wilson-$\theta$ | Bathe |
|---|---|---|---|---|---|
| Span 1 | **−2.768** | −2.743 | −2.737 | −2.751 | −2.743 |
| Span 2 | **−2.100** | −2.079 | −2.119 | −2.086 | −2.082 |
| Span 3 | **−2.055** | −2.093 | −2.052 | −2.028 | −2.094 |
| Span 4 | **−2.061** | −2.083 | −2.057 | −2.043 | −2.074 |
| Span 5 | **−2.060** | −2.053 | −2.058 | −2.037 | −2.052 |
| Span 6 | **−2.068** | −2.024 | −2.058 | −2.060 | −2.030 |
| Span 7 | **−2.110** | −2.100 | −2.105 | −2.129 | −2.111 |
| Span 8 | **−2.745** | −2.746 | −2.746 | −2.757 | −2.727 |

**Table 3**
Maximum displacement values at midspan for each span [mm], as computed by the various numerical time–integration methods using 100 time steps per FE.

| Load position | ENTI | Newmark | HHT-$\alpha$ | Wilson-$\theta$ | Bathe |
|---|---|---|---|---|---|
| Span 1 | **−2.768** | −2.767 | −2.767 | −2.767 | −2.768 |
| Span 2 | **−2.100** | −2.099 | −2.100 | −2.100 | −2.099 |
| Span 3 | **−2.055** | −2.055 | −2.055 | −2.055 | −2.055 |
| Span 4 | **−2.061** | −2.062 | −2.062 | −2.061 | −2.061 |
| Span 5 | **−2.060** | −2.059 | −2.059 | −2.058 | −2.059 |
| Span 6 | **−2.068** | −2.067 | −2.067 | −2.066 | −2.067 |
| Span 7 | **−2.110** | −2.108 | −2.108 | −2.105 | −2.109 |
| Span 8 | **−2.745** | −2.743 | −2.743 | −2.741 | −2.744 |

**Table 4**
Maximum displacement values at midspan for each span [mm], as computed by the various numerical time–integration methods using 1000 time steps per FE.

| Load position | ENTI | Newmark | HHT-$\alpha$ | Wilson-$\theta$ | Bathe |
|---|---|---|---|---|---|
| Span 1 | **−2.768** | −2.768 | −2.768 | −2.768 | −2.768 |
| Span 2 | **−2.100** | −2.100 | −2.100 | −2.100 | −2.100 |
| Span 3 | **−2.055** | −2.055 | −2.055 | −2.055 | −2.055 |
| Span 4 | **−2.061** | −2.061 | −2.061 | −2.061 | −2.061 |
| Span 5 | **−2.060** | −2.060 | −2.060 | −2.059 | −2.060 |
| Span 6 | **−2.068** | −2.068 | −2.068 | −2.068 | −2.068 |
| Span 7 | **−2.110** | −2.110 | −2.110 | −2.110 | −2.110 |
| Span 8 | **−2.745** | −2.745 | −2.745 | −2.745 | −2.745 |

may significantly be influenced by the broad modal frequency spectrum of the structure. High-frequency components that are insufficiently resolved may induce spurious oscillations in non-dissipative schemes or, conversely, be artificially damped when numerical dissipation is introduced.

As previously observed, the differences among the dynamic response variables progressively diminish as the time-step size is reduced.

### 4.2. Comparison of time-domain responses

In this section, the time-domain response of the node located at the midpoint of the first span is investigated, considering displacement, velocity, and acceleration, for the three adopted time steps, equivalent to $n_{steps} = 10, 100, 1000$ per FE. The first 20 s of the simulation correspond to a *forced vibration phase* induced by the ML traversing the beam, while the subsequent 4 s represent a *free vibration phase* after the ML has left the structure.

First two plots (a, b) in Figs. 11–13 show the displacement, velocity, and acceleration time histories obtained with the coarsest time step ($n_{steps} = 10$). Some differences among the numerical schemes are visible, particularly during the free vibration phase. These discrepancies diminish as the time step is reduced, as illustrated in plots (c, d) of the same figures, corresponding to $n_{steps} = 100$ steps per FE. Displacement and velocity profiles are closely aligned across methods, whereas small deviations are observed in the acceleration responses. With the finest time step ($n_{steps} = 1000$ steps per FE), a high level of agreement is achieved for all the response variables, as shown in plots (e, f) of Figs. 11–13, indicating a close agreement among all the numerical results.

Specifically for displacements, Table 5 presents the maximum relative difference in percentages between that calculated by the numerical time-integration schemes and the ENTI method with respect to the maximum value registered by the latter. These differences diminish to 0.01% when adopting a $\Delta t = 8.3125 \cdot 10^{-5}$ s allowing for 1000 steps per FE. This time step size corresponds to a load advancement of 1 mm, which enables a significantly detailed analysis of the structural displacement response. However, for larger models and longer simulations, this time step size may become particularly disadvantageous in terms of computational efficiency and prohibitive burden.

Analogously to displacements, the same analysis is conducted on velocity variables in Table 6. When the ML steps 10 times on a single FE, the error magnifies to 90%, when using the Wilson-$\theta$ method and remains high with the other methods. An increase in the error of about 10% is observed, with respect to the displacement variable, when the time step size is reduced.

Lastly, when investigating the acceleration variables, the error is significantly larger with respect to the other variables, as reported in Table 7 and this aligns with recent findings in the literature, which highlight how standard implicit methods often fail to provide reliable and usable acceleration responses for complex dynamic problems [56]. In fact, the relative error exceeds 100%, due to the presence of short windows where the accelerations calculated with the numerical time-integration schemes exhibit opposite signs, leading to an absolute error greater than the reference maximum value calculated by the ENTI method and used to compute the relative error. Even when employing the finest time step size, the error displays a magnitude in the range of 40–50%, with a lower error obtained with the Bathe method and a greater error with the Wilson-$\theta$ method.

These results demonstrate that acceleration, as being the second derivative of source displacement variable, is particularly sensitive to small phase and amplitude errors in underlying displacement and velocity. Traditional numerical schemes cumulate these errors, which are magnified in the acceleration response. In contrast, the ENTI method inherently addresses this issue by directly evaluating the convolution integral, in an “exact” fashion, provided the time evolution of the force vector is known, thereby producing highly accurate acceleration predictions.

It may be worth emphasizing that the rather hectic oscillations of acceleration responses, made explicitly visible in the time-window zooms in the right column of Fig. 13 (as well as in the earlier space-window zoom in Fig. 10b), look to represent true physical traits, of the real mechanical response, and seem endowed of the full modal content of the discretized model, as duly preserved by the exact nature of the proposed ENTI time-integration strategy. Then, these analytically acquired oscillating responses shall not be linked to spurious artifacts that may be introduced by numerical time-integration techniques (see, for inspectable appreciation, the wider zoom exposed in Fig. 10b).

Main recorded differences, among the undamped structural responses for the 1D FEM upper continuous beam of Paderno d’Adda Bridge, obtained by the ENTI method against the various numerical time-integration techniques, may be recorded among the following, as typical of numerical methods’ shortcomings:

- *Phase shift and period distortion*: traditional implicit and explicit schemes often suffer from period elongation. This numerical artifact causes the computed response to gradually shift out of sync with the exact ENTI reference solution. Since the ENTI method does not introduce any approximation in the evaluation of the calculated response, the natural frequencies and consequently the periods of

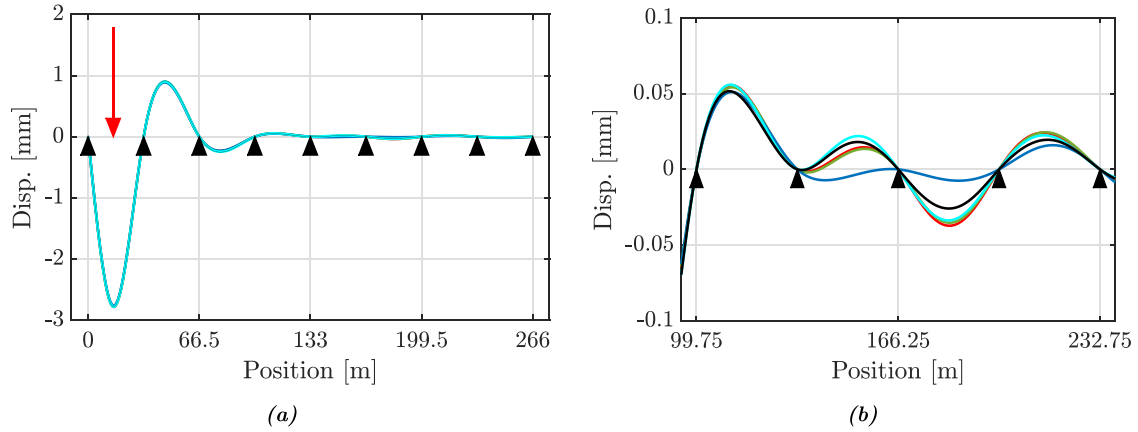



**Fig. 8.** (a) Deformed configuration of the beam at the instant of maximum displacement, computed using the different time-integration schemes: ENTI method (black), Newmark (red), HHT-$\alpha$ (green), Wilson-$\theta$ (blue), and Bathe (cyan), using 10 time steps per FE. (b) Enlarged view of the fourth to seventh spans, highlighting the local differences among the numerical solutions.

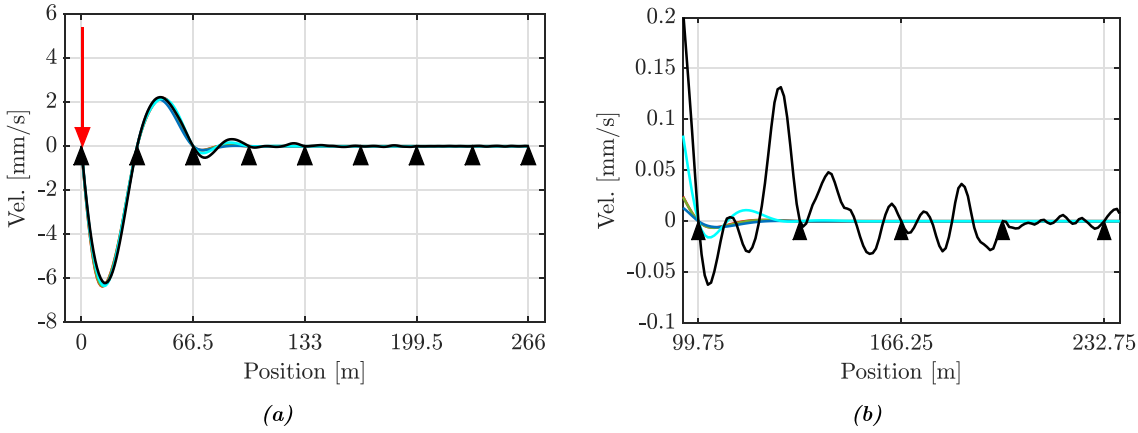



**Fig. 9.** Same as Fig. 8. Velocity field at the instant of maximum velocity.

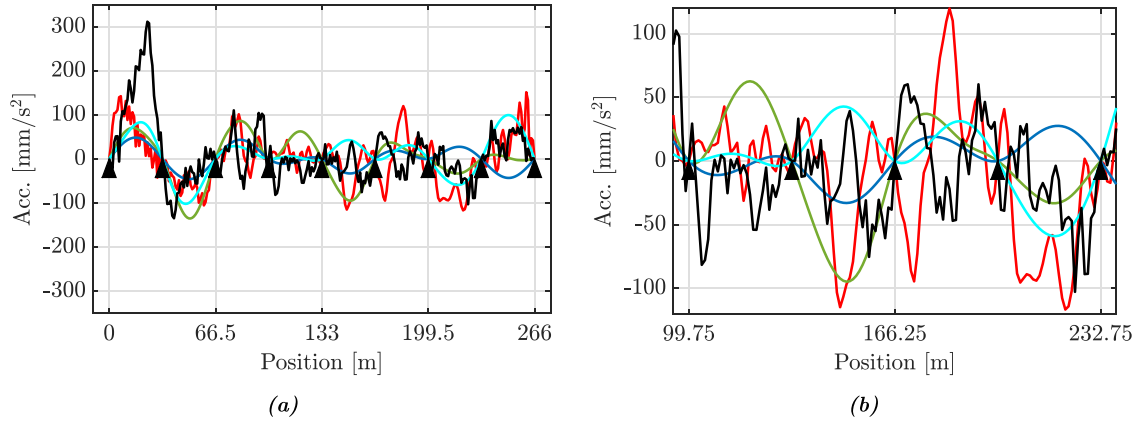



**Fig. 10.** Same as Fig. 8. Acceleration field at the instant of maximum acceleration.

vibration are preserved, ensuring zero phase shift, even over long duration simulations.

- *Artificial damping*: under certain conditions, numerical integrators introduce numerical damping to suppress high-frequency content to remove spurious oscillations, except for Newmark method tuned with average acceleration. However, for undamped systems ($\mathbf{C} = \mathbf{0}$), this leads to a loss of energy during the solution evaluation, which manifests itself as a non-physical decay of oscillation amplitude, as shown for the dynamic variables evaluated with HHT-$\alpha$, Wilson-$\theta$, and Bathe methods. Instead, ENTI, being based on an exact evaluation of the state-transition matrix, namely through the exponential matrix of $\mathbf{S}\Delta t$, perfectly conserves the mechanical energy of the system, in the absence of physical damping.

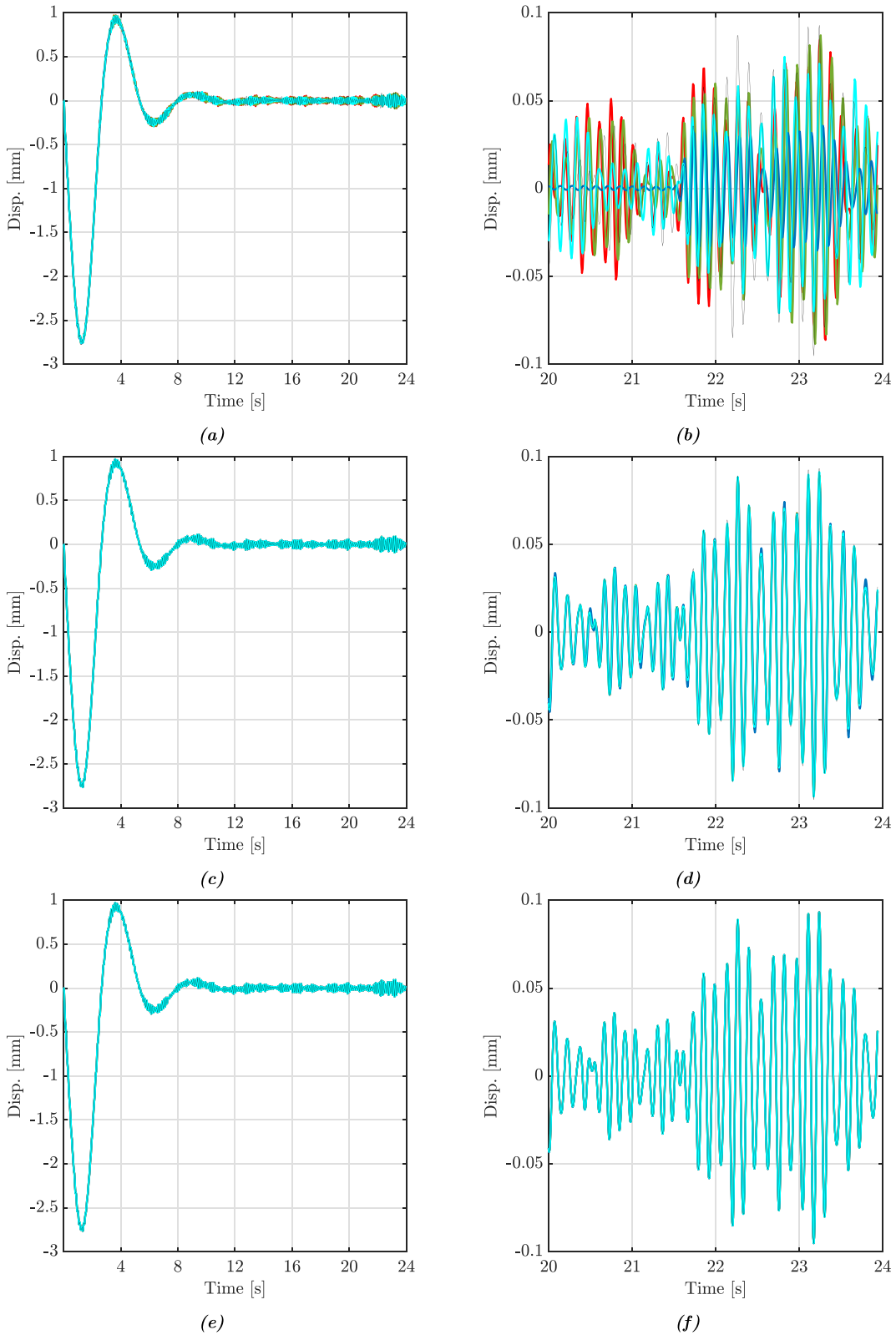



**Fig. 11.** Time history of the displacement of the node at the midpoint of the first span and magnified view of the free vibration phase (between 20 s and 24 s), computed with the various time-integration methods: ENTI (black), Newmark method (red), HHT-$\alpha$ method (green), Wilson-$\theta$ method (blue), and Bathe method (cyan). Plots (a,b) refer to 10 steps per FE, plots (c,d) to 100 steps per FE, plots (e,f) to 1000 steps per FE.

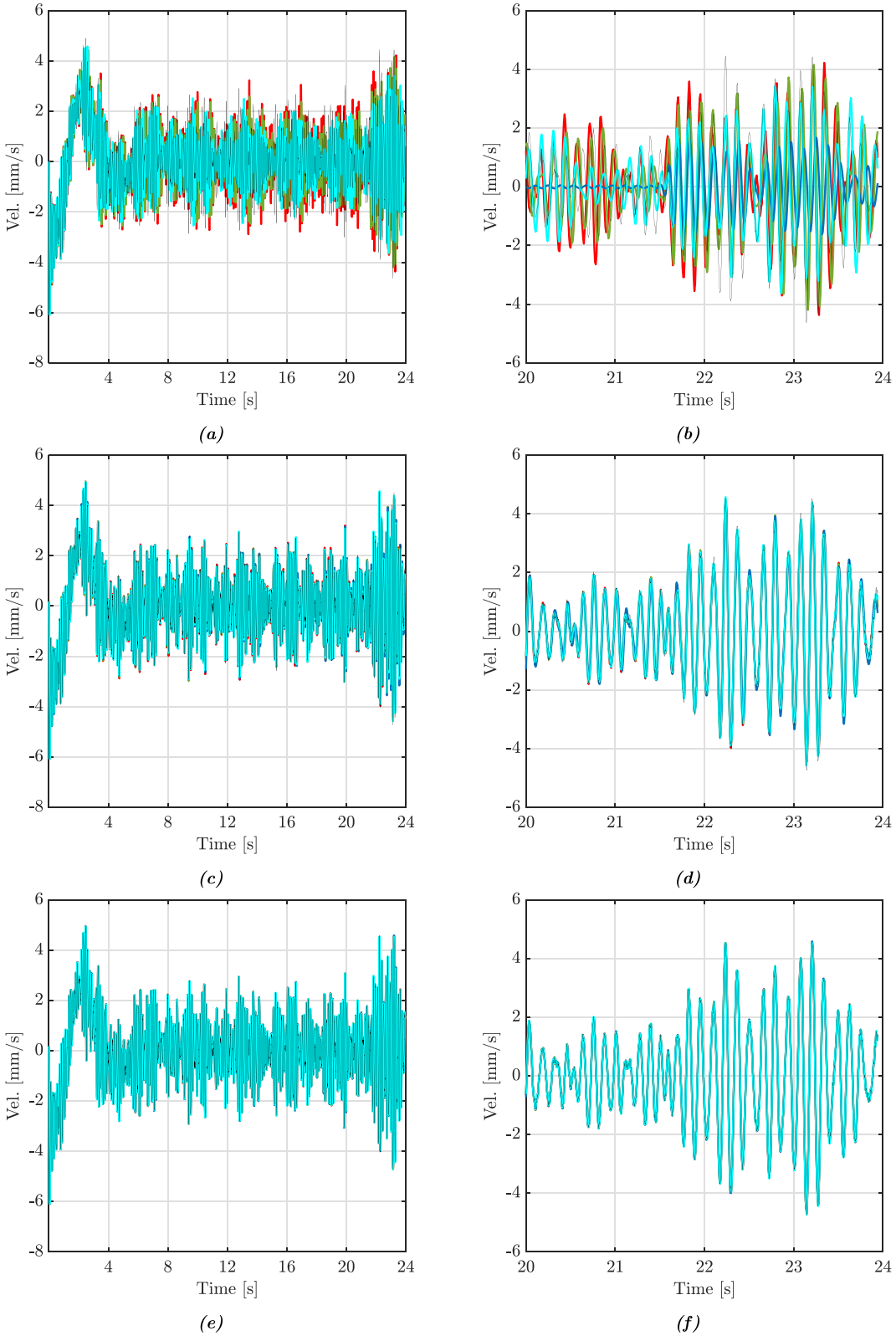



**Fig. 12.** Same as Fig. 11, but for the velocity response of the node at the midpoint of the first span.

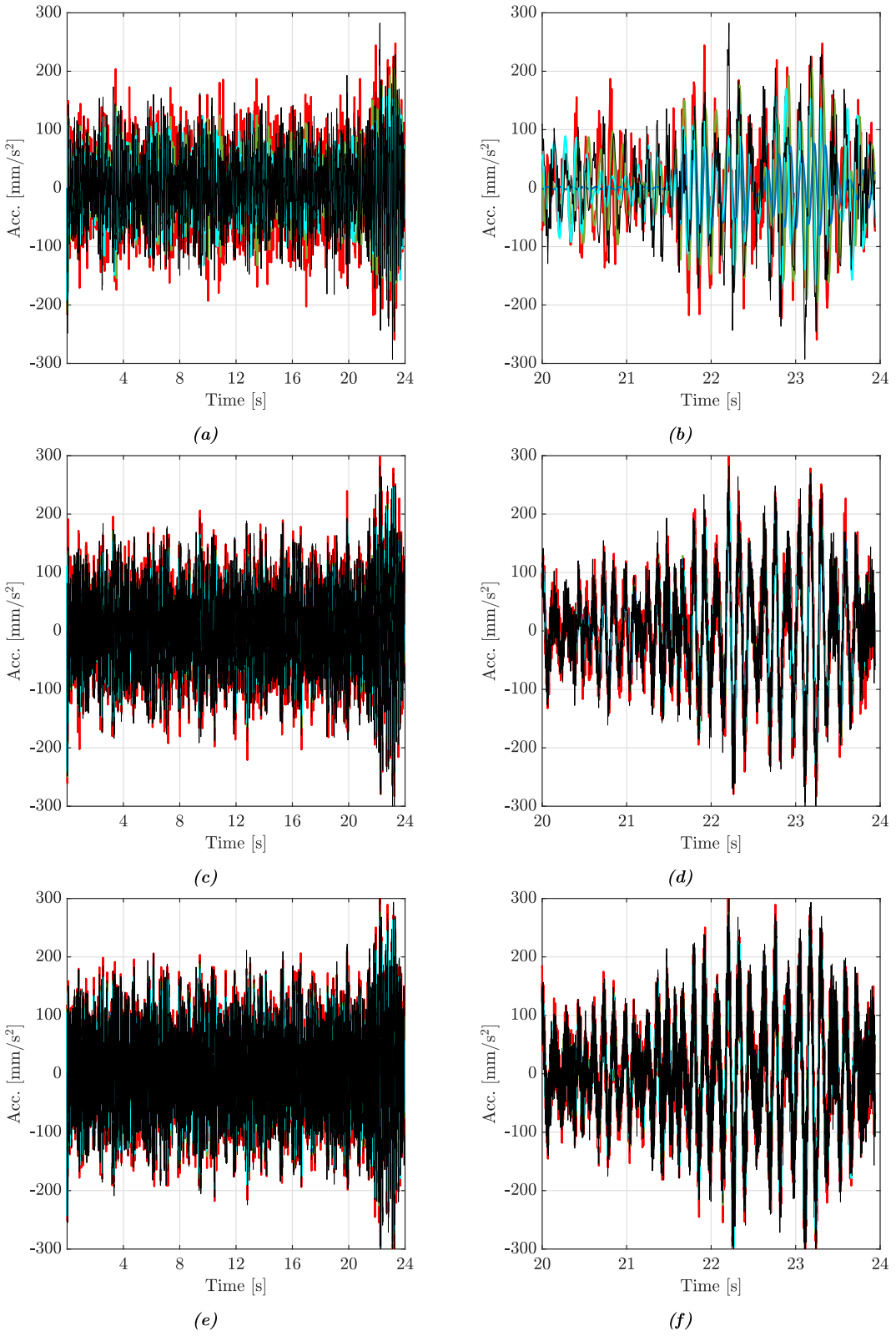



**Fig. 13.** Same as Fig. 11, but for the acceleration response of the node at the midpoint of the first span.

- *Peak cutting*: when the integration time step is not sufficiently small, numerical methods introduce significant truncation errors and numerical damping, which physically prevent the solution from reaching its true extrema. Apparently, the ENTI method for an insufficient size of the time step in the solution representation may also result unable to represent the true extrema in the resulting sampling. However, this phenomenon does not depend on the ENTI method itself as an exact time integration, but is due just to a limited sampling strategy in plotting the evaluated response, with exact values.
- *Computational efficiency and accuracy*: in classical numerical methods, high accuracy requires extremely small time step sizes, increasing the number of operations within the integration loop. Instead, ENTI allows for relatively large time steps, without any loss of accuracy, in both the homogeneous and particular part of the response, leading to a significant optimization for large-scale FEM models. In classical numerical methods, high accuracy and prevention of "overshooting" of physical response shall demand for extreme small time-step sizes.
- *Downsampling feature of ENTI method*: ENTI arises as a natural downsampling method both for intrinsic evaluation (with exact values) and response representation, which may go much beyond what is needed once standard numerical methods are used, necessarily with very fine time steps, in order to achieve precise solutions. As a matter of fact, as stated in Table 8, for the ENTI method the representation of the dynamics variables is exactly reproduced with a time step size of $\Delta t = 8.3125 \cdot 10^{-3}$ s, calculated with $n_{steps} = 10$ per FE, thus requiring about 8.01 s to run the evaluation loop. To achieve the same accuracy in terms of displacement, numerical methods need to be tailored with a finer time step size, about 10 to 100 times shorter and consequently requiring about 16 s for finer $\Delta t$, except for the Bathe method, about 30.66 s. Evaluating the exact solution by using the ENTI method with a time step of $\Delta t = 8.3125 \cdot 10^{-5}$ s requires approximately 800 s. It is important to emphasize that while a coarser sampling obviously captures less high-frequency information due to sampling limits, this does not degrade the mathematical exactness of the solution. Intrinsically to exponential integrators, the homogenous part of the differential equation is exactly evaluated through the state-transition matrix for an arbitrary $\Delta t$ and the ENTI method provides an exact solution even for the non-homogenous part. As a result, instead of computing such a dense structural response, the exact solution is coarsely sampled, thus leading to a reduction of the computational burden.

To provide a clearer representation of these observed response phenomena, various "movies" (evolutive plots) have been generated to fully inspect the dynamic solution in space and time.[1] These animations compare the time-evolution of the structural responses in terms of displacement, velocity and acceleration fields of the 1D FEM beam during the ML passage and the subsequent free vibration phase. Through this type of representation, the aforementioned desynchronization (phase shift) of the numerically calculated responses and the spurious decay of motion in the absence of physical damping can clearly be observed, showing the superiority of the present ENTI exact time-integration strategy.

### 4.3. Salient technical remarks on ENTI application to ML on the bridge beam

The numerical results for the bridge's 1D continuous beam FEM model have been computed by the novel exact ENTI solution and compared against different known numerical methods. Based on this computational analysis, the following main remarks may be drawn:

[1] Such "movies" may be made available as supplementary material to the interested readers, upon request.

**Table 5**
Absolute relative difference of the displacement of the node at the midpoint of the first beam span for different time-step refinements ($n_{steps} = 10, 100, 1000$, i.e., $\Delta t = 8.3125 \cdot 10^{-3}$ s, $8.3125 \cdot 10^{-4}$ s, $8.3125 \cdot 10^{-5}$ s). The error is computed as the maximum absolute difference normalized by the maximum value of the ENTI solution and is expressed as a percentage (%).

| Method | Relative Displacement Error (%) | | |
|---|---|---|---|
| | $n_{steps} = 10$ | $n_{steps} = 100$ | $n_{steps} = 1000$ |
| Newmark | 3.69 | 0.40 | 0.01 |
| HHT-$\alpha$ | 3.35 | 0.43 | 0.01 |
| Wilson-$\theta$ | 4.18 | 0.82 | 0.02 |
| Bathe | 3.24 | 0.19 | 0.01 |

**Table 6**
Same as Table 5. Absolute relative difference of velocities with respect to the maximum value of the ENTI solution, expressed as a percentage (%).

| Method | Relative Velocity Error (%) | | |
|---|---|---|---|
| | $n_{steps} = 10$ | $n_{steps} = 100$ | $n_{steps} = 1000$ |
| Newmark | 83.79 | 12.23 | 2.22 |
| HHT-$\alpha$ | 73.89 | 12.10 | 2.31 |
| Wilson-$\theta$ | 90.06 | 21.35 | 4.06 |
| Bathe | 74.54 | 6.90 | 1.55 |

**Table 7**
Same as Table 5. Absolute relative difference of accelerations with respect to the maximum value of the ENTI solution, expressed as a percentage (%).

| Method | Relative Acceleration Error (%) | | |
|---|---|---|---|
| | $n_{steps} = 10$ | $n_{steps} = 100$ | $n_{steps} = 1000$ |
| Newmark | 105.74 | 68.75 | 48.47 |
| HHT-$\alpha$ | 95.47 | 48.48 | 43.49 |
| Wilson-$\theta$ | 103.67 | 52.12 | 51.62 |
| Bathe | 105.74 | 68.75 | 40.48 |

**Table 8**
Summary of absolute relative errors and computational cost for numerical time-integration schemes with $n_{steps} = 1000$ and exact ENTI solution with $n_{steps} = 10$.

| Method | Disp. Error (%) | Vel. Error (%) | Acc. Error (%) | **CPU Time (s)** |
|---|---|---|---|---|
| **ENTI (Exact)** | – | – | – | **8.01** |
| Newmark | 0.01 | 2.22 | 48.47 | 16.54 |
| HHT-$\alpha$ | 0.01 | 2.31 | 43.49 | 16.07 |
| Wilson-$\theta$ | 0.02 | 4.06 | 51.62 | 15.78 |
| Bathe | 0.01 | 1.55 | 40.48 | 30.66 |

- *Choice of time step size* $\Delta t$. As discussed in Section 3.3, the selection of $\Delta t$ is fundamental, for the accuracy of the numerical time-integration process, while it is only affecting the temporal sampling of the exact response in the ENTI method. Due to the stiff nature of the structure, the effects of high-frequency components exceeding the Nyquist frequency, namely the inverse of the adopted time step, cannot properly be resolved with standard numerical schemes. In particular, the Newmark method, in its non-dissipative form (average acceleration), does not filter out these high frequency contributions, consequently leading to spurious oscillations, much visible in the acceleration responses. Conversely, methods characterized by algorithmic numerical dissipation, such as HHT-$\alpha$, Wilson-$\theta$ or Bathe methods, mitigate this effect, by damping the unresolved high-frequency modes, leading to smoother numerical responses (although possibly failing in other aspects, e.g., phase

shifts, see below). The ENTI method, instead, inherently accounts for the true contribution of each frequency component, in the evaluation of the dynamic response in the time domain.

- *Increase of discrepancies in the ending free vibration phase.* In the forced vibration phase under ML, the displacements calculated with the numerical schemes and with a significantly reduced time step size are characterized by a good agreement, with respect to the exact ENTI solution. When considering instead velocity and particularly acceleration variables, a match of the solution is not properly observed: the Newmark method shows the presence of high frequency components, while the others, specifically the Wilson-$\theta$ method, show an excessive numerical dissipation that tends to aggressively smooth out the solution. However, when the time evolution of the spatial distribution of accelerations is investigated specifically during the subsequent free vibration phase after the ML transit along the beam, for instance, by plotting a "movie" of the solution in space and time (see Footnote 1), more differences emerge. Specifically, the acceleration peaks appear shifted, due to a phase error introduced by the numerical schemes, and occasionally, the response becomes totally out-of-phase. The reason behind this phenomenon shall be related to the wide modal frequency spectrum governing the free vibration phase, which truly challenges the numerical schemes. Recall also that these evidences are herein put to light at zero inherent structural damping, which does not help to calm down the oscillations. To better handle the free-vibration phase, a reduction in (local) time step size may reduce these differences, but this shall lead to a considerable increase in overall computational time and cumulative errors due to spurious effects.
- *Speed of the Moving Load.* In this simulation, the constant-magnitude ML runs over the upper beam at 12.5 m/s, corresponding to 45 km/h, a velocity that was employed in 1889 during the try-out phase of the bridge (SNOS, 1889 [68]). However, nowadays, railway transits are reduced to 15 km/h maximum, due to safety restrictions. Diminishing the travelling speed and adopting the same time step size in the numerical runs leads to an increase in the total number of steps required to complete the simulation. For larger structures and low speed MLs, this may become unfeasible for computational efficiency and, most importantly, accuracy in the obtained results. Differently, the exact ENTI method may be tailored, in terms of sampling, for the model under consideration, to reach a liable trade-off, between computational efficiency and achievable resolution in the dynamic variables' representation.
- *Representation of the dynamic solution.* To better visualize the results and appreciate discrepancies, the evolution of the spatial distribution of the dynamic variables in the time window of interest shall be represented in "movie" form (see Footnote 1). In particular, the differences between the solutions produced by the various time-integration schemes with respect to those calculated using the benchmark exact ENTI method shall become dramatically evident, especially regarding accelerations. Consequently, ENTI-evaluated accelerations shall provide an accurate touchstone to then compare test recordings (e.g., from accelerometers) and numerical simulations within the attempting framework of a reliable digital twin replication.

## 5. Conclusions

This investigation has introduced an Exact Numerical Time Integration (ENTI) method, a novel exponential integration approach, for the accurate structural analysis of discretized dynamic structural systems, in particular under the challenging presence of a Moving Load (ML) dynamic excitation, coupled in space and time. The method enables for the "exact" integration of the equations of motion, by representing the ML as a polynomial function, which allows for a closed-form evaluation of the corresponding convolution integral, through the use of the exponential matrix. Consequently, the computed time-domain responses turn out exact, within the limits of machine precision and any inherent numerical approximations, arising from standard operations and matrix inversion, thereby avoiding numerical errors endemic in conventional time-stepping algorithms.

A fundamental aspect of the present ENTI method is its prior formatting on a state-space formulation, for the structural system at hand. This system representation, through a first-order ODE system becomes advantageous, as a closed-form expression of the solution may be derived and exactly integrated, provided that the external force functions shall allow for an analytical evaluation of the convolution integral. Central to the method is the evaluation of the exponential matrix, which arises from the state-space formulation and is employed to propagate the structural response over time. In undamped (Appendix A) or classically damped (Appendix B) structural systems, this matrix can explicitly be evaluated based on the system's eigenvectors and eigenfrequencies, providing both computational efficiency and analytical transparency. When non-classical structural damping may be present, the exponential matrix may be evaluated in a numerical fashion, via reliable numerical algorithms, provided that their accuracy may carefully be verified, to ensure consistent results across the simulation (see extensive discussions in Sections 3.1.1 and 3.1.2).

The present ENTI method has systematically been applied to a one-dimensional FEM model of the upper continuous beam of the historic Paderno d'Adda Bridge (1889), considering vertical displacements and nodal rotations as DOFs. In this application, a vertical ML of constant magnitude is taken travelling at uniform velocity along the beam, and the corresponding forces are represented as equivalent nodal loads through the third-order polynomial shape functions of standard beam FEs. This modelling captures the essential physical and mechanical features of the ML problem in a discretized structural system, potentially providing a direct link between accurate computational simulations (especially for acceleration responses) and experimental observations (indeed often directly recorded for accelerations).

In particular, the numerical model has been excited using loading conditions resembling those from the original tryouts (in 1889, and 1892) and those from a recent experimental campaign conducted on the bridge structure (May 2024), thereby providing an initial step toward the application of the ENTI method in subsequent, more refined analyses, within the SHM framework of interest, as developed for the historic San Michele Bridge. This actually provided the context and motivation to develop an exact integration method, of the dynamic response, especially in terms of acceleration response variables.

Indeed, the development of the ENTI method was motivated by preliminary analyses using diverse conventional time-integration schemes, which demonstrated substantial discrepancies in displacement, velocity, and particularly acceleration responses, even under highly refined temporal discretizations. These comparisons highlighted the limitations of standard numerical schemes, especially for stiff structures, like the iron San Michele bridge, endowed with a doubly built-in parabolic arch, as meant by the SNOS builder for railway purposes. Consequently, numerical schemes introduce numerical dissipation, overshooting and phase errors, which become especially pronounced in the acceleration responses, due to its augmented sensitivity to small errors in displacement and velocity. The ENTI method, in contrast, provides an exact solution, for Linear Time-Invariant systems, with polynomially-defined loads, offering a reliable benchmark for evaluating conventional numerical algorithms and forming an efficient and affordable tool, removing unwanted numerical errors.

This is achieved by the proposed ENTI strategy, independently of the time-step size, which is basically selected just to achieve an appropriate sampling of the exact solution representation. This shall allow for a considerable reduction of computational burden, especially over large time windows of dynamic analysis, anyway reaching a superior accuracy, with respect to standard numerical schemes, which shall anyhow

require rather fine time discretizations, to achieve reasonable solution representations.

Another important contribution of this work shall lie in the optimized computational implementation of the ENTI method. By pre-computing all matrices and vectors that are independent of the assumed constant time step, including the core exponential matrix operator and the polynomial load coefficients, the method confines the mathematical operations within the time-stepping loop, to simply state updates and acceleration evaluations. This strategy reduces the computational cost and minimizes the accumulation of round-off errors. Furthermore, a rigorous assessment of the exponential matrix accuracy in undamped and classically damped systems has been provided, showing that the ENTI approach remains robust, across a wide range of temporal discretizations and can safely be applied to practical engineering problems.

Notice, moreover, that the present work shall present significant advances in both numerical (a), and basic and specific mechanics (b) aspects, in the considered context of exponential exact time integration and Moving Load excitation. Specifically, the following remarks may be in order.

(a) Numerical aspects:
- On time-integration numerical relevance, the accuracy of the dynamic solution shall present a genuine relevance, especially once acceleration responses are of a chief interest, significantly in SHM contexts, where accelerations may typically be acquired by accelerometer sensors.
- Still on that, moreover, the whole time-integration procedure is carried out in closed-form, eliminating any time-integration truncation errors. This shall be considered as a rather significant contribution, as most exponential integrators still rely on numerical quadrature, to treat forcing terms. This is herein bypassed in a ML propagation case, since the integration of the forcing term is led by third-order polynomials, making of course specific the case that is handled in the study. However, in principle, this may later be generalized to other excitation contexts, specifically on measured load histories (which may require hybrid strategies, for merging a numerical quadrature forcing term with the analytical integral of the homogeneous solution, as other exponential integrators may do), for the various specific cases under consideration.

(b) Mechanics aspects:
- On basic and specific mechanics aspects, the considered mechanical context, of Moving Load excitation on a continuous 1D beam, and particular application toward the analysis of the upper continuous beam of San Michele Bridge (1889), brings important novelty in terms of the understanding of the physical processes involved in the dynamic response under ML, and provides a clear visualization in nearing the response observation of the bridge's beam, as it may be registered by acquired response signals. Toward a final close matching among modelling prediction and experimental recordings, it has been felt and demonstrated that the present proposal of time-integration evaluation clearly overcomes typical limitations of conventional numerical time-integration schemes.
- Specifically on that, one may emphasize that the model-acquired accelerations, with marked hectic oscillations, shall reproduce, as preserved by the present ENTI method, the full modal and dynamic content of the mechanical system, with respect to classical outcomes from known numerical schemes, as exposed in the paper.

In summary, the present novel ENTI method shall constitute a general and problem-specific, highly accurate, computationally efficient time-integration framework, particularly for the ML analysis of discretized (FEM) structural models. Relative to conventional numerical time-stepping schemes, the ENTI method departs from a black-box paradigm, adopting instead a tailored formulation that yields exact time-domain responses. The method is broadly applicable to Linear Time-Invariant systems, and its scope may be extended to more complex dynamic excitations, still in the present one-dimensional Euler-Bernoulli beam context, or in other possible single- or multi-dimensional structural scenarios, such as, for instance, 2D plates or 2D/3D truss-frame models (Ferrari et al. [71,72]), and considering different other-than-FEM discretized or naturally discrete modelization contexts. Moreover, future developments shall focus on merging such developments within SHM frameworks and platforms, under development, providing a robust computational tool that shall bridge precise numerical modelling with practical monitoring and assessment of historic and modern structures and infrastructures.

## CRediT authorship contribution statement

**Michele Guerini:** Writing – original draft, Methodology, Investigation, Data curation, Conceptualization. **Rosalba Ferrari:** Writing – review & editing, Supervision, Methodology, Investigation, Funding acquisition, Conceptualization. **Giuseppe Cocchetti:** Writing – review & editing, Supervision, Methodology, Investigation, Data curation, Conceptualization. **Egidio Rizzi:** Writing – review & editing, Supervision, Methodology, Investigation, Conceptualization.

## Declaration of competing interest

The authors declare that they have no known competing financial interests or personal relationships that could have appeared to influence the work reported in this paper.

## Acknowledgements

This research was supported by the Italian Ministry of University and Research (MUR) under the PRIN 2022 program (funding following reallocation of resources from the final ranking), Project Code 2022744YM9, CUP F53C24000930006, as well as by institutional research funds ("Fondi di Ricerca d'Ateneo ex 60%") and a doctoral grant at the University of Bergamo.

## Appendix A. Exponential matrix in the undamped case

In this appendix, the analytical expression of exponential matrix $e^{-\mathbf{S}(t-t_0)}$ is derived for an undamped structural system, $\mathbf{C} = \mathbf{0}$, characterized by symmetric and positive definite mass matrix $\mathbf{M}$ and stiffness matrix $\mathbf{K}$, under free vibrations:

$$\mathbf{M\ddot{u}} + \mathbf{Ku} = \mathbf{0} \tag{34}$$

The derivation involves solving the above second-order system through a projection into the principal reference system, mapping back the solution to the physical reference system and eventually comparing the resulting displacement and velocity vectors with a first-order state-space solution.

The mapping between principal $\mathbf{p}(t)$ and physical $\mathbf{u}(t)$ coordinates is defined as:

$$\mathbf{u}(t) = \mathbf{\Phi p}(t) \tag{35}$$

where $\mathbf{\Phi}$ represents the matrix of column-eigenvectors. By exploiting the orthogonality properties of the eigenvectors (e.g., by choosing a normalization with $\mathbf{\Phi}^{\mathrm{T}}\mathbf{M\Phi} = \mathbf{I}$ and $\mathbf{\Phi}^{\mathrm{T}}\mathbf{K\Phi} = \mathbf{\Omega}^2$, where $\mathbf{\Omega}^2 = \mathrm{diag}(\omega_1^2, \ldots, \omega_n^2)$ contains the eigenvalues), the system is expressed in principal coordinates, thus Eq. (34) is decoupled into $n$ independent equations. In matrix form, the following expression yields:

$$\ddot{\mathbf{p}} + \mathbf{\Omega}^2\mathbf{p} = \mathbf{0} \tag{36}$$

Modal response $\mathbf{p}(t)$ is then calculated by the superposition of effects as:

$$\mathbf{p}(t) = \cos\Big(\mathbf{\Omega}(t-t_0)\Big)\mathbf{c}_1 + \sin\Big(\mathbf{\Omega}(t-t_0)\Big)\mathbf{c}_2 \tag{37}$$

Constant vectors $\mathbf{c}_1$ and $\mathbf{c}_2$ are determined by imposing the initial conditions in principal coordinates, $\mathbf{p}(t_0) = \mathbf{p}_0$ and $\dot{\mathbf{p}}(t_0) = \dot{\mathbf{p}}_0$. These values are obtained by projecting the physical initial conditions, $\mathbf{u}_0$ and $\dot{\mathbf{u}}_0$, into the principal domain through the relationships $\mathbf{p}_0 = \boldsymbol{\Phi}^{\mathrm{T}}\mathbf{M}\mathbf{u}_0$ and $\dot{\mathbf{p}}_0 = \boldsymbol{\Phi}^{\mathrm{T}}\mathbf{M}\dot{\mathbf{u}}_0$. This procedure leads to the following expressions for the coefficients:

$$\mathbf{c}_1 = \mathbf{p}_0 \tag{38}$$

$$\mathbf{c}_2 = \boldsymbol{\Omega}^{-1}\dot{\mathbf{p}}_0 \tag{39}$$

The state vector collecting both principal displacements and velocities vectors may then be expressed as a matrix product between the state-transition matrix and the initial state vector, yielding:

$$\begin{bmatrix}\mathbf{p}(t)\\ \dot{\mathbf{p}}(t)\end{bmatrix} = \begin{bmatrix}\mathbf{G}_{11}(t-t_0) & \mathbf{G}_{12}(t-t_0)\\ \mathbf{G}_{21}(t-t_0) & \mathbf{G}_{22}(t-t_0)\end{bmatrix}\begin{bmatrix}\mathbf{p}_0\\ \dot{\mathbf{p}}_0\end{bmatrix} \tag{40}$$

where $\mathbf{G}_{ij}(t-t_0)$ are herein called modal time-evolution matrix functions and are defined as block-diagonal matrix functions providing the link between the initial conditions and the current state.

In this undamped case, once constants $\mathbf{c}_1$ and $\mathbf{c}_2$ in Eqs. (39) are substituted into Eq. (37), displacement modal time-evolution matrix functions $\mathbf{G}_{11}(t-t_0)$ and $\mathbf{G}_{12}(t-t_0)$ are identified as:

$$\mathbf{G}_{11}(t-t_0) = \cos\Big(\boldsymbol{\Omega}(t-t_0)\Big) \tag{41a}$$

$$\mathbf{G}_{12}(t-t_0) = \boldsymbol{\Omega}^{-1}\sin\Big(\boldsymbol{\Omega}(t-t_0)\Big) \tag{41b}$$

Given the expression for principal displacements vector $\mathbf{p}(t)$ from Eq. (37), where constants $\mathbf{c}_1$ and $\mathbf{c}_2$ are made explicit with Eqs. (39), principal velocities vector $\dot{\mathbf{p}}(t)$ is evaluated by differentiating $\mathbf{G}_{11}(t-t_0)$ and $\mathbf{G}_{12}(t-t_0)$:

$$\dot{\mathbf{p}}(t) = \dot{\mathbf{G}}_{11}(t)\,\mathbf{p}_0 + \dot{\mathbf{G}}_{12}(t)\,\dot{\mathbf{p}}_0 \tag{42}$$

Consequently, modal time-evolution matrix functions $\mathbf{G}_{21}(t-t_0)$ and $\mathbf{G}_{22}(t-t_0)$ for the velocity vector may be evaluated by differentiating the modal time-evolution matrix functions of the displacement vector:

$$\mathbf{G}_{21}(t-t_0) = \dot{\mathbf{G}}_{11}(t-t_0) = -\boldsymbol{\Omega}\sin\Big(\boldsymbol{\Omega}(t-t_0)\Big) \tag{43a}$$

$$\mathbf{G}_{22}(t-t_0) = \dot{\mathbf{G}}_{12}(t-t_0) = \cos\Big(\boldsymbol{\Omega}(t-t_0)\Big) = \mathbf{G}_{11}(t-t_0) \tag{43b}$$

By mapping principal state vector $\mathbf{p}(t)$ back to physical domain $\mathbf{u}(t)$ through Eq. (35) and comparing resulting nodal displacements $\mathbf{u}(t)$ and velocities $\dot{\mathbf{u}}(t)$ with state-space formulation expressed as $\mathbf{z}(t) = \mathrm{e}^{-\mathbf{S}(t-t_0)}\mathbf{z}_0$, with $\mathbf{z} = [\mathbf{u}(t)^{\mathrm{T}},\ \dot{\mathbf{u}}(t)^{\mathrm{T}}]^{\mathrm{T}}$, the block-partitioned structure of the exponential matrix in the undamped case is directly identified:

$$\mathrm{e}^{-\mathbf{S}(t-t_0)} = \begin{bmatrix}\boldsymbol{\Phi} & \mathbf{0}\\ \mathbf{0} & \boldsymbol{\Phi}\end{bmatrix}\begin{bmatrix}\mathbf{G}_{11}(t-t_0) & \mathbf{G}_{12}(t-t_0)\\ \mathbf{G}_{21}(t-t_0) & \mathbf{G}_{22}(t-t_0)\end{bmatrix}\begin{bmatrix}\boldsymbol{\Phi}^{\mathrm{T}}\mathbf{M} & \mathbf{0}\\ \mathbf{0} & \boldsymbol{\Phi}^{\mathrm{T}}\mathbf{M}\end{bmatrix} \tag{44}$$

This representation highlights that the components of the exponential matrix are explicitly determined by the independent solutions of the displacement and velocity vectors.

## Appendix B. Exponential matrix in the classically damped case

As a generalization of the treatment in Appendix A, for undamped systems, $\mathbf{C} = \mathbf{0}$, the derivation can be extended to linear viscous damped systems, assuming classical damping, allowing for decoupling also matrix $\mathbf{C}$. This condition assumes that damping matrix $\mathbf{C}$ displays the same eigenvectors as mass $\mathbf{M}$ and stiffness $\mathbf{K}$ matrices, in the unforced damped equations of motion:

$$\mathbf{M}\ddot{\mathbf{u}} + \mathbf{C}\dot{\mathbf{u}} + \mathbf{K}\mathbf{u} = \mathbf{0} \tag{45}$$

As for the derivation in Appendix A, the same normalization properties of eigenvectors are assumed to hold ($\boldsymbol{\Phi}^{\mathrm{T}}\mathbf{M}\boldsymbol{\Phi} = \mathbf{I}$ and $\boldsymbol{\Phi}^{\mathrm{T}}\mathbf{K}\boldsymbol{\Phi} = \boldsymbol{\Omega}^2$).

For classical damping, the projection of the solution into the principal reference system, $\mathbf{u} = \boldsymbol{\Phi}\mathbf{p}$, using real eigenvector matrix $\boldsymbol{\Phi}$, simultaneously diagonalizes all dynamic matrices. Specifically, the damping matrix also satisfies the orthogonality condition:

$$\boldsymbol{\Phi}^{\mathrm{T}}\mathbf{C}\boldsymbol{\Phi} = 2\mathbf{Z}\boldsymbol{\Omega} \tag{46}$$

where $\mathbf{Z} = \mathrm{diag}(\zeta_1, \ldots, \zeta_n)$ contains the modal damping ratios. This property again allows the coupled system to be decomposed into $n$ independent scalar equations, expressed in matrix form as:

$$\ddot{\mathbf{p}} + 2\mathbf{Z}\boldsymbol{\Omega}\dot{\mathbf{p}} + \boldsymbol{\Omega}^2\mathbf{p} = \mathbf{0} \tag{47}$$

Assuming a subcritically damped system ($0 \le \zeta_i < 1$ for all the principal modes), the response is governed by the damped natural frequencies defined by diagonal matrix $\boldsymbol{\Omega}_d = \boldsymbol{\Omega}(\mathbf{I} - \mathbf{Z}^2)^{1/2}$. Indeed, displacement $\mathbf{p}(t)$ in principal coordinates may be formulated in terms of an exponentially decaying amplitude:

$$\mathbf{p}(t) = \mathrm{e}^{-\mathbf{Z}\boldsymbol{\Omega}(t-t_0)}\left(\mathrm{e}^{j\boldsymbol{\Omega}_d(t-t_0)}\mathbf{c}_1 + \mathrm{e}^{-j\boldsymbol{\Omega}_d(t-t_0)}\mathbf{c}_2\right) \tag{48}$$

where $j$ is the imaginary unit, and $\mathbf{c}_1, \mathbf{c}_2$ are constant vectors to be determined from initial conditions $\mathbf{u}(t_0) = \mathbf{u}_0$ and $\dot{\mathbf{u}}(t_0) = \dot{\mathbf{u}}_0$. The initial conditions in principal coordinates $\mathbf{p}_0 = \mathbf{p}(t_0)$ and principal velocity $\dot{\mathbf{p}}_0 = \dot{\mathbf{p}}(t_0)$ are determined by extracting $\mathbf{p}(t)$ from Eq. (35) at $t = t_0$, as for the undamped system. By evaluating Eq. (48) and its time derivative at the initial time, the following linear system is obtained:

$$\mathbf{c}_1 + \mathbf{c}_2 = \mathbf{p}_0 \tag{49}$$

$$j\boldsymbol{\Omega}_d(\mathbf{c}_1 - \mathbf{c}_2) = \dot{\mathbf{p}}_0 + \mathbf{Z}\boldsymbol{\Omega}\mathbf{p}_0 \tag{50}$$

Solving for constants $\mathbf{c}_1$, $\mathbf{c}_2$ yields a conjugate pair of complex coefficient vectors:

$$\mathbf{c}_{1,2} = \frac{1}{2}\left[\mathbf{p}_0 \mp j\boldsymbol{\Omega}_d^{-1}\left(\dot{\mathbf{p}}_0 + \mathbf{Z}\boldsymbol{\Omega}\mathbf{p}_0\right)\right] \tag{51}$$

By replacing constants $\mathbf{c}_1$ and $\mathbf{c}_2$ into Eq. (48) and applying Euler's formula of complex numbers, the solution is expressed in terms of damped sine and cosine matrix functions:

$$\mathbf{p}(t) = \mathrm{e}^{-\mathbf{Z}\boldsymbol{\Omega}(t-t_0)}\left\{\left[\cos\Big(\boldsymbol{\Omega}_d(t-t_0)\Big) + \mathbf{Z}\boldsymbol{\Omega}\boldsymbol{\Omega}_d^{-1}\sin\Big(\boldsymbol{\Omega}_d(t-t_0)\Big)\right]\mathbf{p}_0 + \boldsymbol{\Omega}_d^{-1}\sin\Big(\boldsymbol{\Omega}_d(t-t_0)\Big)\dot{\mathbf{p}}_0\right\} \tag{52}$$

The solution in principal coordinates, expressed by Eq. (52) is rearranged and expressed as a combination of initial displacement $\mathbf{p}_0$ and velocity $\dot{\mathbf{p}}_0$:

$$\mathbf{p}(t) = \mathbf{G}_{11}(t-t_0)\mathbf{p}_0 + \mathbf{G}_{12}(t-t_0)\dot{\mathbf{p}}_0 \tag{53}$$

where time-dependent diagonal matrices $\mathbf{G}_{11}(t-t_0)$ and $\mathbf{G}_{12}(t-t_0)$ represent the damped displacement modal time-evolution matrix functions:

$$\mathbf{G}_{11}(t-t_0) = \mathrm{e}^{-\mathbf{Z}\boldsymbol{\Omega}(t-t_0)}\left[\cos\Big(\boldsymbol{\Omega}_d(t-t_0)\Big) + \mathbf{Z}\boldsymbol{\Omega}\boldsymbol{\Omega}_d^{-1}\sin\Big(\boldsymbol{\Omega}_d(t-t_0)\Big)\right] \tag{54a}$$

$$\mathbf{G}_{12}(t-t_0) = \mathrm{e}^{-\mathbf{Z}\boldsymbol{\Omega}(t-t_0)}\boldsymbol{\Omega}_d^{-1}\sin\Big(\boldsymbol{\Omega}_d(t-t_0)\Big) \tag{54b}$$

To obtain the complete state response, principal velocity vector $\dot{\mathbf{p}}(t)$ is derived by differentiating the operators above. This leads to the definition of the damped velocity modal time-evolution matrix functions:

$$\mathbf{G}_{21}(t-t_0) = \dot{\mathbf{G}}_{11}(t-t_0) = -\mathrm{e}^{-\mathbf{Z}\boldsymbol{\Omega}(t-t_0)}\boldsymbol{\Omega}^2\boldsymbol{\Omega}_d^{-1}\sin\Big(\boldsymbol{\Omega}_d(t-t_0)\Big) \tag{55a}$$

$$\mathbf{G}_{22}(t-t_0) = \dot{\mathbf{G}}_{12}(t-t_0) = \mathrm{e}^{-\mathbf{Z}\boldsymbol{\Omega}(t-t_0)}\left[\cos\Big(\boldsymbol{\Omega}_d(t-t_0)\Big) - \mathbf{Z}\boldsymbol{\Omega}\boldsymbol{\Omega}_d^{-1}\sin\Big(\boldsymbol{\Omega}_d(t-t_0)\Big)\right] \tag{55b}$$

Exponential matrix $\mathrm{e}^{-\mathbf{S}(t-t_0)}$ for the classically damped system then follows the same block-partitioned formulation as in Eq. (44), using the corresponding damped modal time-evolution matrix functions. Notice that, for the undamped case, $\mathbf{C} = \mathbf{0}$, i.e., $\mathbf{Z} = \mathbf{0}$, the modal time-evolution matrix functions and the resulting exponential matrix reduce to those in Appendix A.

## Data availability

No data were used for the research described in the article.

## References


[1] Ferrari R, Rizzi E. On the theory of the ellipse of elasticity as a natural discretisation method in the design of Paderno d'Adda Bridge (Italy). In: D'Ayala D, Fodde E, editors. Structural analysis of historic construction: preserving safety and significance (SAHC08). London: CRC Press, Taylor & Francis Group; 2008. p. 583–91. https://doi.org/10.1201/9781439828229

[2] Ferrari R, Cocchetti G, Rizzi E. Computational elastoplastic Limit Analysis of the Paderno d'Adda bridge (Italy, 1889). Arch Civ Mech Eng 2018;18(1):291–310. https://doi.org/10.1016/j.acme.2017.05.002

[3] Ferrari R, Rizzi E, Brioschi MS, Dertimanis VK. Design of an effective structural health monitoring platform for Paderno d'Adda Bridge (1889). In: Sementsov S, Leontyev A, Huerta S, editors. Reconstruction and restoration of architectural heritage 2021. London: CRC Press, Taylor & Francis Group; 2021. p. 210–5. https://doi.org/10.1201/9781003136804-41

[4] Su X, Zhang Q, Li Y, Huang Y, Jia Z. Damage identification of a jacket platform based on a hybrid deep learning framework. Struct Health Monit 2025;24(3):1700–24. https://doi.org/10.1177/14759217241262558

[5] Vrtač T, Ocepek D, Česnik M, Čepon G, Boltežar M. A hybrid modeling strategy for training data generation in machine learning-based structural health monitoring. Mech Syst Signal Process 2024;207(15 January 2024):110937. https://doi.org/10.1016/j.ymssp.2023.110937

[6] Bao Y, Tang Z, Li H, Zhang Y. Computer vision and deep learning–based data anomaly detection method for structural health monitoring. Struct Health Monit 2018;18(2):401–21. https://doi.org/10.1177/1475921718757405

[7] Stoura CD, Dimitrakopoulos EG. A Modified Bridge System method to characterize and decouple vehicle–bridge interaction. Acta Mech 2020;231(9):3825–45. https://doi.org/10.1007/s00707-020-02699-3

[8] Yang YB, Yang JP. State-of-the-art review on modal identification and damage detection of bridges by moving test vehicles. Int J Struct Stab Dyn 2018;18(2):1850025. https://doi.org/10.1142/S0219455418500256

[9] Stoura CD, Greś S, Dertimanis VK, Ancu L, Chatzi EN. Identification of railway bridge modal properties based solely on acceleration data from traversing trains. Mech Syst Signal Process 2025;239:113342. https://doi.org/10.1016/j.ymssp.2025.113342

[10] Yang JP, Chen LH. A two-span vehicle-bridge interaction system integrating a two-axle vehicle for vehicle scanning method. Eng Struct 2026;346:121599. https://doi.org/10.1016/j.engstruct.2025.121599

[11] Froio D, Rizzi E, Simões FMF, Pinto da Costa A. Universal analytical solution of the steady-state response of an infinite beam on a Pasternak elastic foundation under moving load. Int J Solids Struct 2018;132–133(February 2018):245–63. https://doi.org/10.1016/j.ijsolstr.2017.10.005

[12] Froio D, Rizzi E, Simões FMF, Pinto da Costa A. Dynamics of a beam on a bilinear elastic foundation under harmonic moving load. Acta Mech 2018;229(10):4141–65. https://doi.org/10.1007/s00707-018-2213-4

[13] Froio D, Verzeroli L, Ferrari R, Rizzi E. On the numerical modelization of moving load beam problems by a dedicated parallel computing FEM implementation. Arch Comput Methods Eng 2021;28(4):2253–314. https://doi.org/10.1007/s11831-020-09459-5

[14] Cha YJ, Ali R, Lewis J, Büyüköztürk O. Deep learning-based structural health monitoring. Autom Constr 2024;161:105328. https://doi.org/10.1016/j.autcon.2024.105328

[15] Zheng W, Li J, Hao H, Fan G. Missing data imputation for structural health monitoring using unsupervised domain adaptation and pretraining techniques. Eng Struct 2025;328(1 April 2025):119694. https://doi.org/10.1016/j.engstruct.2025.119694

[16] Ravizza G, Ferrari R, Rizzi E, Chatzi EN. Effective Heterogeneous Data Fusion procedure via Kalman filtering. Smart Struct. Syst. 2018;22(5):631–41. https://doi.org/10.12989/sss.2018.22.5.631

[17] Ravizza G, Ferrari R, Rizzi E, Dertimanis V. On the denoising of structural vibration response records from low-cost sensors: a critical comparison and assessment. J Civ Struct Health Monit 2021;11(5):1201–24. https://doi.org/10.1007/s13349-021-00502-y

[18] Newmark N. A method of computation for structural dynamics. J. Eng. Mech. Div. ASCE 1959;85(3):67–94. https://doi.org/10.1061/JMCEA3.0000098

[19] Wilson EL. A computer program for the dynamic stress analysis of underground structures. SESM Report No. 68-1. Berkeley: Division of Structural Engineering Structural Mechanics, University of California; 1968.

[20] Bathe KJ, Wilson EL. Stability and accuracy analysis of direct integration methods. Earthq Eng Struct Dyn 1972;1(3):283–91. https://doi.org/10.1002/eqe.4290010308

[21] Hilber HM, Hughes TJ, Taylor RL. Improved numerical dissipation for time integration algorithms in structural dynamics. Earthq Eng Struct Dyn 1977;5(3):283–92. https://doi.org/10.1002/eqe.4290050306

[22] Hughes TJR. Analysis of transient algorithms with particular reference to stability behavior. In: Belytschko T, Hughes TJR, editors. Computational methods for transient analysis. Amsterdam: North-Holland; 1983. p. 67–155.

[23] Chung J, Hulbert G. A time integration algorithm for structural dynamics with improved numerical dissipation: the generalized-α method. J Appl Mech 1993;60(2):371–5. https://doi.org/10.1115/1.2900803

[24] Bathe KJ, Baig MMI. On a composite implicit time integration procedure for nonlinear dynamics. Comput Struct 2005;83(31–32):2513–24. https://doi.org/10.1016/j.compstruc.2005.08.001

[25] Bathe KJ, Noh G. Insight into an implicit time integration scheme for structural dynamics. Comput Struct 2012;98-99(May 2012):1–6. https://doi.org/10.1016/j.compstruc.2012.01.009

[26] Benítez JM, Montáns FJ. The value of numerical amplification matrices in time integration methods. Comput Struct 2013;128(November 2013):243–50. https://doi.org/10.1016/j.compstruc.2013.07.001

[27] Bahar LY, Sinha AK. Matrix exponential approach to dynamic response. Comput Struct 1975;5(2–3):159–65. https://doi.org/10.1016/0045-7949(75)90006-1

[28] Hochbruck M, Ostermann A. Exponential integrators. Acta Numer 2010;19:209–86. https://doi.org/10.1017/S0962492910000048

[29] Hersch J. Contribution à la méthode des équations aux différences. Z. für angew. Math. Phys. ZAMP 1958;9:129–80. https://doi.org/10.1007/BF01600630

[30] Certaine J. The solution of ordinary differential equations with large time constants. In: Ralston A, Wilf HS, editors. Mathematical methods for digital computers. New York: Wiley; 1960. p. 128–32.

[31] Pope DA. An exponential method of numerical integration of ordinary differential equations. Commun. Assoc. Comput. Mach. 1963;6(8):491–3. https://doi.org/10.1145/366707.367592

[32] Tokman M, Loffeld J. Efficient design of exponential-Krylov integrators for large scale computing. Procedia Comput Sci 2010;1(1):229–37. https://doi.org/10.1016/j.procs.2010.04.026

[33] Loffeld J, Tokman M. Comparative performance of exponential, implicit, and explicit integrators for stiff systems of ODEs. J Comput Appl Math 2013;241(15 March 2013):45–67. https://doi.org/10.1016/j.cam.2012.09.038

[34] Knoll DA, Keyes DE. Jacobian-free Newton–Krylov methods: a survey of approaches and applications. J Comput Phys 2004;193(2):357–97. https://doi.org/10.1016/j.jcp.2003.08.010

[35] Lin J, Shen W, Williams FV. A high precision direct integration scheme for structures subjected to transient dynamic loading. Comput Struct 1995;56(1):113–20. https://doi.org/10.1016/0045-7949(94)00537-D

[36] Michels LD, Sobottka GA, Weber AG. Exponential integrators for stiff elastodynamic problems. ACM Trans Graph 2014;33(1):1–20. https://doi.org/10.1145/2508462

[37] Pari P, Kanungo B, Gavini V. Exponential time propagators for elastodynamics. J Mech Phys Solids 2024;193:105871. https://doi.org/10.1016/j.jmps.2024.105871

[38] Magnus W. On the exponential solution of differential equations for a linear operator. Commun Pure Appl Math 1954;7(4):649–73. https://doi.org/10.1002/cpa.3160070404

[39] Blanes S, Casas F, Oteo JA, Ros J. The Magnus expansion and some of its applications. Phys Rep 2009;470(5–6):151–238. https://doi.org/10.1016/j.physrep.2008.11.001

[40] Lu YY. Computing a matrix function for exponential integrators. J Comput Appl Math 2003;161(1):203–16. https://doi.org/10.1016/j.cam.2003.08.006

[41] Wang MF, Ftk A. On the precise integration methods based on Padé approximations. Comput Struct 2009;87(5–6):380–90. https://doi.org/10.1016/j.compstruc.2008.11.004

[42] Sastre J, Ibáñez J, Defez E, Ruiz P. New scaling-squaring Taylor algorithms for computing the matrix exponential. SIAM J Sci Comput 2015;37(1):439–55. https://doi.org/10.1137/090763202

[43] Ruiz P, Sastre J, Ibáñez J, Defez E. High performance computing of the matrix exponential. J Comput Appl Math 2016;291(January 2016):370–9. https://doi.org/10.1016/j.cam.2015.04.001

[44] Wu F, Zhang K, Zhu L, Hu J. High-performance computation of the exponential of a large sparse matrix. SIAM J Matrix Anal Appl 2020;42(4):1636–55. https://doi.org/10.1137/20M1342987

[45] Calandrini S, Pieper K, Gunzburger MD. Exponential time differencing for the tracer equations appearing in primitive equation ocean models. Comput Methods Appl Mech Eng 2020;365:113002. https://doi.org/10.1016/j.cma.2020.113002

[46] Song C, Eisenträger S, Zhang X. High-order implicit time integration scheme based on Padé expansions. Comput Methods Appl Mech Eng 2022;390:114436. https://doi.org/10.1016/j.cma.2021.114436

[47] Fryba L. Vibration of solids and structures under moving loads. 3rd ed. London: Thomas Telford; 1999. https://doi.org/10.1680/vosasuml.35393

[48] Santos HAFA. A new finite element formulation for the dynamic analysis of beams under moving loads. Comput Struct 2024;298:107347. https://doi.org/10.1016/j.compstruc.2024.107347

[49] Beskos DE, Boley BA. Use of dynamic influence coefficients in forced vibration problems with the aid of Laplace transform. Comput Struct 1975;5(5–6):263–9. https://doi.org/10.1016/0045-7949(75)90030-9

[50] Manolis GD, Beskos DE. Thermally induced vibrations of beam structures. Comput Methods Appl Mech Eng 1980;21(3):337–55. https://doi.org/10.1016/0045-7825(80)90101-2

[51] Narayanan GV, Beskos DE. Dynamic soil-structure interaction by numerical Laplace transform. Eng. Struct. 1982;4(1):53–62. https://doi.org/10.1016/0141-0296(82)90024-4

[52] Narayanan GV, Beskos DE. Numerical operational methods for time-dependent linear problems. Int. J. Numer. Methods 1982;18(12):1829–54. https://doi.org/10.1002/nme.1620181207

[53] Spyrakos CC, Beskos DE. Dynamic response of flexible strip-foundations by boundary and finite elements. Soil Dyn Earthq Eng 1986;5(2):84–96. https://doi.org/10.1016/0267-7261(86)90002-3

[54] Tamma KK, Spyrakos CC, Lambi MA. Thermal/structural dynamic analysis via a transform-method-based finite-element approach. J Spacecr Rockets 1987;24(3):219–26. https://doi.org/10.2514/3.25902

[55] Kang S, Bui-Thanh T. A scalable exponential-DG approach for nonlinear conservation laws: with application to Burger and Euler equations. Comput Methods Appl Mech Eng 2021;385:114031. https://doi.org/10.1016/j.cma.2021.114031

[56] O'Shea D, Zhang X, Mohammadian S, Song C. A high-order implicit time integration method for linear and nonlinear dynamics with efficient computation of accelerations. Comput Methods Appl Mech Eng 2025;438:117831. https://doi.org/10.1016/j.cma.2025.117831
[57] Coddington EA, Levinson N. Theory of ordinary differential equations. New York: McGraw-Hill; 1955.
[58] Boyce WE, DiPrima RC, Meade DB. Elementary differential equations and boundary value problems. 11th ed. Hoboken: Wiley; 2017.
[59] Rugh WJ. Linear system theory. 2nd ed. Upper Saddle River: Prentice-Hall; 1996.
[60] Hartman P. Ordinary differential equations. 2nd ed. Philadelphia: Society for Industrial and Applied Mathematics (SIAM); 2002.
[61] MathWorks. MATLAB documentation. Available at: https://www.mathworks.com/help. (Accessed 2026).
[62] Moler C, Van Loan C. Nineteen dubious ways to compute the exponential of a matrix, twenty-five years later. SIAM Rev 2003;45(1):3–49. https://doi.org/10.1137/S00361445024180
[63] Niesen J, Wright WM. Algorithm 919: a Krylov subspace algorithm for evaluating the ϕ-functions appearing in exponential integrators. ACM Trans Math Softw 2012;38(3):1–22. https://doi.org/10.1145/2168773.2168781
[64] Al-Mohy AH, Higham NJ. Computing the action of the matrix exponential, with an application to exponential integrators. SIAM J Sci Comput 2011;33(2):488–511. https://doi.org/10.1137/100788860
[65] Ferrari R, Cocchetti G, Rizzi E. Reference structural investigation on a 19th-century arch iron bridge loyal to design-stage conditions. Int J Archit Herit 2020;14(10):1425–55. https://doi.org/10.1080/15583058.2019.1613453
[66] Gentile C, Saisi A. Ambient vibration testing and condition assessment of the Paderno iron arch bridge (1889). Constr Build Mater 2011;25(9):3709–20. https://doi.org/10.1016/j.conbuildmat.2011.04.019
[67] Guerini M, Ferrari R, Cocchetti G, Rizzi E. Effective numerical time integration of structural dynamic responses under Moving Load. In: Milani G, Magagnini E, Khatir S, editors. Proceedings of the 4th international conference of steel and composite for engineering structures (ICSCES 2025). Lecture Notes in Civil Engineering, vol. 746. Cham: Springer; 2025. p. 734–47. https://doi.org/10.1007/978-3-032-04350-4_62
[68] Società Nazionale delle Officine di Savigliano. Viadotto di Paderno sull'Adda (Ferrovia Ponte S. Pietro-Seregno). Torino: Tip. e Lit. Camilla e Bertolero; 1889.
[69] Ermolli L, Guerini M, Stoura CD, Ferrari R, Dertimanis VK, Chatzi EN, Rizzi E. Combining experimental data and numerical modeling to analyze train-structure interaction on the historic San Michele Bridge (Italy, 1889). In: Papadrakakis M, Papadopoulos V, Stefanou G, editors. 6th ECCOMAS thematic conference on uncertainty quantification in computational science and engineering (UNCECOMP 2025), Rhodes Island, Greece, June 15–18, 2025. Proceeding ID: 21526. p. 266–77. https://doi.org/10.7712/120225.12355.21526
[70] Guerini M, Ermolli L, Stoura CD, Ferrari R, Dertimanis VK, Chatzi EN, Rizzi E. Modal dynamic identification of historic San Michele Bridge (Italy, 1889). In: Papadrakakis M, Fragiadakis M, editors. 10th ECCOMAS thematic conference on computational methods in structural dynamics and earthquake engineering (COMPDYN 2025), Rhodes Island, Greece, June 15–18, 2025. Proceeding ID: 26049. p. 4923–36. https://doi.org/10.7712/120125.12784.26049
[71] Ferrari R, Cocchetti G, Rizzi E. Limit Analysis of a historical iron arch bridge. Formulation and computational implementation. Comput Struct 2016;175(October 2016):184–96. https://doi.org/10.1016/j.compstruc.2016.05.007
[72] Ferrari R, Cocchetti G, Rizzi E. Effective iterative algorithm for the Limit Analysis of truss-frame structures by a kinematic approach. Comput Struct 2018;197(February 2018):28–41. https://doi.org/10.1016/j.compstruc.2017.11.018